Activation of human TLR4/MD-2 by hypoacylated lipopolysaccharide from a clinical isolate of Burkholderia cenocepacia

Di Lorenzo, F., Kubik, Ł., Oblak, A., Lorè, N. I., Cigana, C., Lanzetta, R., Parrilli, M., Hamad, M. A., De Soyza, A., Silipo, A., Jerala, R., Bragonzi, A., Valvano, M. A., Martín-Santamaría, S., & Molinaro, A. (2015). Activation of human TLR4/MD-2 by hypoacylated lipopolysaccharide from a clinical isolate of Burkholderia cenocepacia. *Journal of Biological Chemistry*, *290*(35), 21305-21319. https://doi.org/10.1074/jbc.M115.649087

Published in:
Journal of Biological Chemistry

Document Version:
Peer reviewed version

JBC Papers in Press. Published on July 9, 2015 as Manuscript M115.649087
The latest version is at http://www.jbc.org/cgi/doi/10.1074/jbc.M115.649087

Activation of human TLR4/MD-2 by hypoacylated lipopolysaccharide from a clinical isolate of *Burkholderia cenocepacia**

Flaviana Di Lorenzo[1,4], Łukasz Kubik[2,3], Alja Oblak[4,5], Nicola Ivan Lorè[6], Cristina Cigana[6], Rosa Lanzetta[1], Michelangelo Parrilli[1], Mohamad A. Hamad[7], Anthony De Soyza[8], Alba Silipo[1], Roman Jerala[4,5], Alessandra Bragonzi[6], Miguel A. Valvano[7,9], Sonsoles Martín-Santamaría[2,10*], and Antonio Molinaro[1*]

[1] Department of Chemical Sciences, University of Naples Federico II, Naples 80126, Italy.

[2] Department of Chemistry and Biochemistry, Universidad CEU San Pablo, Boadilla del Monte, Madrid 28668, Spain.

[3] Department of Biopharmaceutics and Pharmacodynamics, Medical University of Gdańsk, Gdańsk 80-416, Poland.

[4] Department of Biotechnology, National Institute of Chemistry, Ljubljana 1000, Slovenia.

[5] Centre of excellence EN-FIST, Ljubljana 1000, Slovenia.

[6] Infection and Cystic Fibrosis Unit, IRCCS - San Raffaele Scientific Institute, Milan 20132, Italy

[7] Department of Microbiology and Immunology, University of Western Ontario, London N6A 5C1, Canada.

[8] Applied Immunobiology and Transplantation Group, Institute of Cellular Medicine, University of Newcastle, Newcastle NE1 7RU, United Kingdom.

[9] Centre for Infection and Immunity, Queen's University Belfast, Belfast BT9 7AE, United Kingdom

[10] Current address: Department of Chemical and Physical Biology, Centre for Biological Research, CIB-CSIC, Madrid 28040, Spain.

*Running title: *Activation of TLR4/MD-2 by Burkholderia LPS*

* To whom correspondence should be addressed: Antonio Molinaro, Department of Chemical Sciences, University of Naples Federico II, 80126, Naples, Italy. Tel.: (0039) 081674123; Fax: (0039) 081674393; E-mail: molinaro@unina.it. Sonsoles Martín-Santamaría, Department of Chemical and Physical Biology, Centre for Biological Research, CIB-CSIC, 28040, Madrid, Spain. Tel.: (0034) 0918373112; Fax: (0034) 915360432; E-mail: smsantamaria@cib.csic.es

Keywords: Innate immunity; Lipopolysaccharide (LPS); Cystic Fibrosis; *Burkholderia*; TLR4/MD-2 complex

Background: The *Burkholderia cenocepacia* lipid A is hypoacylated.
Results: Aminoarabinose residues in lipid A contribute to *Burkholderia* lipid A binding to the TLR4/MD-2 complex.
Conclusion: A novel mode of *Burkholderia* lipopolysaccharide-TLR4/MD-2 interactions promotes inflammation.
Significance: Modifications of the lipid A structure enhance pro-inflammatory responses of hypoacylated lipopolysaccharide.

ABSTRACT

Lung infection by *Burkholderia* species, in particular *B. cenocepacia*, accelerates tissue damage and increase post-lung transplant mortality in cystic fibrosis patients. Host-microbes interplay largely depends on interactions between pathogen specific molecules and innate immune receptors such as the Toll-like receptor 4 (TLR4), which recognizes the lipid A moiety of the bacterial lipopolysaccharide (LPS). The human TLR4/MD-2 LPS receptor complex is strongly activated by hexa-acylated lipid A and poorly activated by underacylated lipid A. Here, we report that *B. cenocepacia* LPS strongly activates human TLR4/MD-2 despite its lipid A having only five acyl chains. Further, we show that aminoarabinose residues in lipid A contribute to TLR4-lipid A interactions, and experiments in a mouse model of LPS-induced endotoxic shock confirmed the pro-inflammatory potential of *B. cenocepacia* penta-acylated lipid A. Molecular modeling, combined with mutagenesis of TLR4-MD2 interactive surfaces, suggests that longer acyl chains and the aminoarabinose residues in the *B. cenocepacia* lipid A allow exposure of the fifth acyl chain on the surface of MD-2 enabling interactions with TLR4 and its dimerization. Our results provide a molecular model for activation of the human TLR4/MD-2 complex by penta-acylated lipid A, explaining the ability of hypoacylated *B. cenocepacia* LPS to promote pro-inflammatory responses associated to the severe pathogenicity of this opportunistic bacterium.

A central theme in innate immunity involves recognition of conserved microbial molecules (pathogen-associated molecular patterns) by surface receptors expressed on phagocytic cells (1,2). Pathogen recognition triggers cell signaling cascades leading to activation of transcription factors such as nuclear factor-κB (NF-κB) and interferon regulatory factors (IRFs), which in turn stimulate production of inflammatory cytokines (e.g. TNF-α, IL-1β, and type I interferons) (3). Lipopolysaccharide (LPS), the major component of the Gram-negative bacterial outer membrane, elicits potent innate immune responses through interactions with a receptor complex composed of Toll-like receptor 4 (TLR4) and the myeloid differentiation factor 2 (MD-2) (4). Depending on the amount and chemical nature of LPS released from the pathogen, TLR4/MD-2 recognition stimulates a protective immune response or leads to uncontrolled inflammation associated with high mortality (5,6). LPS is a complex glycolipid consisting of three distinct domains (Fig. 1) (7): lipid A, core oligosaccharide, and in many bacteria, a repeating polysaccharide moiety known as the O-antigen (8-10). Lipid A, composed of an acylated glucosamine disaccharide backbone, is the LPS moiety recognized by the TLR4/MD-2 receptor complex. Lipid A bioactivity depends on its chemical structure. The number and distribution of acyl chains, and the presence of the phosphate groups in the di-glucosamine backbone determine the agonistic and antagonistic activities of lipid A (11-19). Most enteric bacteria, such as *Escherichia coli*, produce hexa-acylated *bis*-phosphorylated lipid A, which has the highest cytokine-inducing capacity in mammals. In contrast, tetra-acylated lipid A (as lipid IV_A) and most of penta-acylated lipid A forms lack activity on human cells (19,20).

Lipid A interacts with a hydrophobic pocket formed by two anti-parallel β-sheets of MD-2 mediating the dimerization and activation of the TLR4/MD-2 complex (19,21). The MD-2 hydrophobic pocket can accommodate up to five acyl chains. For agonistic hexa-acylated *E. coli* lipid A, five acyl chains are buried within the pocket while the sixth chain lies on a channel of the MD-2 surface, building a hydrophobic region and the dimerization interface required for interaction with the TLR4 partner (referred to here as TLR4*). This arrangement enables hydrophobic interactions bridging the

TLR4/MD-2/LPS heterodimer and promoting the juxtaposition of the intracellular domains leading to activation of signal transduction (18,22). By contrast, antagonist lipid IV_A binds to human MD-2 with all four acyl chains completely buried in the hydrophobic pocket precluding dimerization and subsequent activation (23). Similarly, many penta-acylated lipid As act as an antagonist of human TLR4/MD-2 (24-25). In contrast, lipid IV_A can activate the murine TLR4/MD-2 complex (26).

Bacteria regulate the degree of lipid A acylation in response to environmental conditions. For example, *Pseudomonas aeruginosa* strains possess penta-acylated lipid A, but can produce hexa-acylated lipid A during infection in cystic fibrosis (CF) patients (27), gaining the ability to elicit stronger inflammation. Intriguingly, the non-CF pathogen *Porphyromonas gingivalis* produces a high heterogeneous LPS lipid A whose penta-acylated isoform potently activates the NF-kB pathway in human gingival fibroblasts in a similar manner to the *E. coli* LPS (28). Therefore, the molecular mechanisms underlying TLR4 dimerization and activation cannot always be predicted based on the *E. coli* lipid A-TLR4/MD2 paradigm.

Burkholderia cenocepacia is an opportunistic Gram-negative bacterium causing serious infections in CF patients (29). Understanding how *B. cenocepacia* infection elicits inflammation is crucial to find new ways to improve treatment of infected CF patients. The structure of the *B. cenocepacia* LPS (LPS_{BC}) was previously described (30). The lipid A moiety of LPS_{BC} consists of a mixture of penta-acylated and tetra-acylated, *bis*-phosphorylated di-glucosamine backbone with two 4-amino-4-deoxy-L-arabinose (L-Ara4N) residues linked by phosphodiester linkages (Fig. 1) (30). The acyl chains are made of 3-(*R*)-hydroxyhexadecanoic acid C16:0 (3-OH), 3-(*R*)-hydroxytetradecanoic acid C14:0 (3-OH) and hydroxytetradecanoic acid C14:0 (Fig. 1) (30). The L-Ara4N decoration of lipid A is essential for *B. cenocepacia* viability (31) and represents the major determinant of resistance to cationic antimicrobial peptides (30,31). The structural features of LPS_{BC} suggest the molecule would be a very poor TLR4/MD-2 complex agonist compared to the prototypic enterobacterial LPS. In contrast, several studies show that LPS_{BC}, as well as biological and synthetic lipid A analogues, is highly pro-inflammatory (32-36). Therefore, the current model for binding/activation of human TLR4/MD-2 complex cannot explain why LPS_{BC} is pro-inflammatory. In this work, we investigated the molecular basis of the mechanism of LPS_{BC} recognition and report for the first time that longer acyl chains than those in enterobacterial lipid A together with the L-Ara4N residues allow *B. cenocepacia* lipid A (LA_{BC}) to fit into the binding pocket of MD-2 in a manner that promotes TLR4 dimerization, leading to activation of inflammatory responses in cellular and animal models.

EXPERIMENTAL PROCEDURES

LPS extraction and purification–LPS was prepared from *B. cenocepacia* strains MH71 and MH75 (30). Both strains are isogenic derivatives of the K56-2 clinical isolate and contain a deletion of the *wbiF* gene that eliminates O-antigen production. MH75 has also a deletion removing genes involved in UDP-L-Ara4N synthesis and therefore cannot produce LPS with L-Ara4N residues ($LPS_{BC\Delta Ara}$). Both MH71 and MH75 also carry a suppressor mutation in the LPS transport gene *lptG* that allows for the transport of LPS devoid of L-Ara4N to the bacterial outer membrane (30). The *P. aeruginosa* RP73 clinical isolate was obtained from a chronically infected CF patient and kindly provided by Prof. Burkhard Tümmler (Klinische Forschergruppe, Medizinische Hochschule Hannover, Germany) (37,38). Strains were plated on trypticase soy agar (TSA) plates and cultured in trypticase soy broth (TSB) at 37 °C. For large-scale LPS purification, bacteria were treated with hot phenol/water (39). After extensive dialysis against distilled water, the extracted phases were subjected to enzymatic digestions to remove nucleic acids and protein contaminants. Water and phenol fractions were analyzed by 13.5% SDS-PAGE and silver

staining (40). The LPS fraction was exclusively found in the water phase.

Isolation of lipid A–Lipid A was obtained by hydrolysis of the LPS with 100 mM sodium acetate buffer pH 4.4, (100°C, 3 h). The solution was extracted three times with $CHCl_3$/MeOH/H_2O (100:100:30 v/v/v) and centrifuged (4°C, 5000 x *g*, 15 min). The organic phase contained lipid A and the water phase contained the core oligosaccharide. The former was further purified through several washes with distilled water and then liophilized. The lipid A and core oligosaccharide structures of strains K56-2, MH71 and MH75 were characterized elsewhere (Fig. 1) (30,41).

Mice endotoxic studies–Animal studies were conducted according to protocols approved by San Raffaele Scientific Institute (Milan, Italy) Institutional Animal Care and Use Committee (IACUC) and adhered strictly to the Italian Ministry of Health guidelines for the use and care of experimental animals. Efforts were made to minimize the number of animals used and their suffering. C57BL/6 mice, 20-22 g male (Charls River) were challenged via intraperitoneal (i.p.) injection with 300 μg/mouse of LPS from *E. coli* and *P. aeruginosa* RP73, LPS_{BC}, and $LPS_{BC\Delta Ara}$. Control mice were challeged with sterile saline solution. Five hours after treatment, mice were sacrificed by CO_2 administration, and blood collected from heart puncture. The blood clot was left at room temperature for 15-30 min. The clot was removed by centrifugation at 2,000 x *g* for 10 min at 4°C. Sera were collected and stored at -20 °C. TNF-α concentration in sera was determined by ELISA (R&D Systems), according to manufacturer instructions using antibody pairs and recombinant standards from R&D System.

HEK293 cell activation and luciferase reporter assays–Expression plasmids containing sequences of human TLR4, MD-2 and the pELAM-1 firefly luciferase plasmid were a gift from Dr. C. Kirschning (Technical University of Munich, Germany). Expression plasmid containing sequence of mouse TLR4 was purchased from InvivoGen (CA, USA). Expression plasmid for mouse MD-2 was a gift from Dr. Y. Nagai (University of Tokyo, Japan). The Renilla luciferase phRL-TK plasmid was purchased from Promega (WI, USA). Recombinant MD-2 genes were cloned into pEF-BOS with Flag and His tags on the C-terminus. Recombinant TLR4 genes were cloned into pUNO with a C-terminal HA tag. Transfection reagent JetPEI was purchased from Polyplus-Transfection (France) and was used according to the manufacturer's instructions. The human embryonic kidney (HEK) 293 cells were provided by Dr. J. Chow (Eisai Research Institute, Andover, USA) and grown in DMEM supplemented with 10 % FBS. The MD-2 mutants were made using QuikChange site-directed mutagenesis kit (Stratagene, USA) according to the manufacturer's instructions. All plasmids were sequenced to confirm the appropriate mutations. For the NF-κB-luciferase reporter assay, HEK293 cells were seeded in 96-well plates at 3 x 10^4 cells/well and incubated overnight in a humidified atmosphere (5% CO_2) at 37 °C. The next day, when cells were 60-80% confluent, they were co-transfected with the plasmids for MD-2 (10 ng), TLR4 (1 ng), NF-κB-dependent luciferase (50 ng) and constitutive Renilla luciferase (10 ng) using JetPEI transfection reagent (all amounts are in ng/well). Cells were stimulated 6 h after transfection with endotoxin preparations. Cells were lysed after 16 h of stimulation in 1x reporter assay lysis buffer (Promega, USA) and analysed for reporter gene activities using a dual-luciferase reporter assay system. Relative luciferase units (RLU) were calculated by normalizing each sample's luciferase activity for constitutive Renilla activity measured within the same sample.

Statistical analysis–Results were expressed as mean±S.D from experiments done in triplicate. Statistical calculations and tests *in vitro* and *in vivo* were performed using Student's t test considering $P \leq 0.05$ as limit of statistical significance and a P value of 0.001 extremely significant.

Molecular modeling: building and geometry optimization of LPS_{BC} and $LPS_{BC\Delta Ara}$–3-D

coordinates were built by Maestro (42). Molecular mechanics optimization (UFF force field), semi-empirical calculations (AM1), and DFT (B3LYP/6-31G*) were subsequently applied using Gaussian03 (43). Ammonium and carboxylic acid groups were considered as ionized. Conformational analysis on DS1, DS2 and DS3 disaccharides was performed with Macromodel (44). The parameters were: MM3* force field, water solvent constant dielectric, dielectric constant of 1.0. The charges from the force field were employed, with an extended cut-off. The best conformers were selected, and from them molecular dynamics simulations (MDS) with implicit water and MM3* as force field, were performed using Schrödinger Maestro 9.3 Impact 5.8 (42,45) (MM3* force field, dielectric constant: 80.0 number of MDS steps 100, time step (ps) 0,001).

The full 3D structures of $LA_{BC\Delta Ara}$, LA_{BC}, and LPS_{BC} were built with Maestro, using optimized disaccharide scaffolds obtained from the conformational analysis. FA chains, DS6 and amino-arabinoses were optimized separately using Gaussian 03 (B3LYP/6-31G*). Starting conformation for lipid A optimization was obtained from *E. coli* lipid A from PDB 3fxi. Full structure of LPS_{BC} was built by putting together core region disaccharides and lipid A with five aliphatic chains. Final MDS of the geometry was performed with implicit water by means of Impact (MM3* force field, dielectric constant: 80.0, number of MDS steps 100, time step (ps) 0,001). 3D Structures of lipid A molecules for validation were extracted from their corresponding PDB files (*E. coli* lipid A was obtained from PDB 3fxi, and Re chemotype of *E. coli* lipid A from PDB 3vq2), refined with the help of Maestro, and finally submitted to MDS with Impact (MM3* force field, and implicit water).

Molecular modeling–For docking studies with MD-2 and TLR4 proteins, 3D coordinates from MD-2 protein were obtained from PDB 3fxi (human MD-2) and 3vq2 (murine MD-2), and refined and minimized with the Protein Preparation Wizard module of Maestro, using amber force field (46). The TLR4 structure was obtained from PDB 3fxi, and treated following the same procedure after removing water molecules and any other non-standard residue.

Two different docking methodologies were used for docking studies of $LA_{BC\Delta Ara}$ and LA_{BC} on MD-2: AutoDock and AutoDock Vina. While AutoDock is a widely used semi-empirical docking method (47), the recently released AutoDock Vina combines empirical and knowledge-based scoring functions, with good performance and reduced computing time (48). Each ligand was docked into human and murine MD-2 protein using AutoDock 4.2 (49), and separately using AutoDock Vina 1.1.2. (48). For human MD-2 (from PDB 3fxi), the Autogrid grid point spacing was set at 0.375 Å, center coordinates of the grid box were 29.00, -7.00, 17.875(x, y, z), and number of grid points in xyz was 41, 53, 83. For murine MD-2 (from PDB 3vq2), the Autogrid grid point spacing was set at 0.375 Å, center coordinates of the grid box were -27.50, -15.50, 22.00 (x, y, z), leading to with 75 x 40 x 60 (x, y, z) grid points. The best result from each docking job with LA_{BC} was used as starting geometry for subsequent docking calculations. Different combinations of allowed rotatable bonds were also considered for the ligands. Docking calculations with AutoDock were performed using Genetic Algorithm (number of individuals in population 150, maximum number of energy evaluations 2500000-5000000, maximum number of generations 27000, number of top individuals to survive to next generation 1, rate of gene mutation 0.02, rate of crossover 0.8, window size 10, Alpha parameter of Cauchy distribution 0.0, Beta parameter Cauchy distribution 1.0). When docking LPS_{BC}, flexible docking was also performed considering Asp101, Glu120 and Glu122 as flexible residues. Docking calculations with AutoDock Vina were also performed. Coordinates and dimensions of grid boxes, starting geometries and general methodology were the same as for AutoDock. When docking LPS_{BC}, flexible docking was also performed considering Asp101 as flexible residue. 3D structures of the docked complexes

were optimized by MDS with Impact (implicit water, and AMBER* force field).

For docking experiments studies of the *B. cenocepacia* LPS core on human TLR4 we used AutoDock Vina 1.1.2. Torsional bonds from the ligand were allowed to rotate. Ammonium groups were considered as ionized. Grid box was built on TLR4 from PDB 3fxi with grid center at 26.00, -22.00, 11.50 (x, y, z), number of grid points of 41 x 41 x 43 (x, y, z), and spacing of 0.375 Å. Final optimization of the 3D structure of the docked complex was carried out by MDS with Impact (implicit water, and AMBER* force field).

The full complex of human TLR4/MD-2 with *B. cenocepacia* LPS core was built by merging docked MD-2/LPS core complex with docked LPS inner core/TLR4 using PDB 3fxi as template. The resulting structure was optimized by MDS with implicit water (AMBER* force field). Coupling of two TLR4/MD-2/LPS_{BC} complexes was finally performed also using PDB 3fxi as template. The full 3D structure of the dimer complex was submitted to MDS with implicit water and AMBER* force field (charges from: force field, cut-off: extended, method: PRCG, maximum iterations: 500, converge on: gradient, convergence threshold: 0.05). This final structure for the TLR4/MD-2/LPS_{BC} complex was used to generate the mutant TLR4/MD-2/LPS_{BC} complex (D294A, R322A, S415A*, and S416A*) by changing the corresponding side chains to Ala side chain. The resulting structure was submitted to MDS with implicit water and AMBER* force field. Energy analysis was performed by means of the MM-ISMSA method (50).

RESULTS

LPS and lipid A from B. cenocepacia activate the TLR4/MD-2 complex and have pro-inflammatory activity in vivo–TLR4/MD-2 activation by LPS_{BC} and LA_{BC} was examined using the NF-κB reporter luciferase assay in transiently transfected HEK293 and HEK293T cells co-expressing murine or human MD-2 (mMD-2, hMD-2) and murine or human TLR4 (mTLR4, hTLR4). Initial results revealed that LPS_{BC} and LA_{BC} activate both human and mouse TLR4/MD-2 complexes (Figs. 2, 3*A* and 3*B*). Since LA_{BC} possesses longer acyl chains than those in *E. coli* lipid A and constitutively carries one or two L-Ara4N residues, to further understand the structure-function relationship of LPS_{BC}, we utilized LPS from a mutant strain lacking the ability to produce L-Ara4N ($LPS_{BC\Delta Ara}$). NF-κB reporter luciferase assays demonstrated that at 5 ng/ml, LPS_{BC} and $LPS_{BC\Delta Ara}$ induced activation of TLR4/MD-2 complexes (Fig. 2). Similar results were obtained in dose-response experiments with purified LA_{BC} and $LA_{BC\Delta Ara}$ (at 5, 10, and 50 ng/ml) in cells co-expressing mTLR4/mMD-2 and hTLR4/hMD-2 (Figs 3*A* and 3*B*, respectively), which also demonstrated consistent agonistic activity at the lowest concentration of 5 ng/ml. However, NF-κB activation by mouse (Fig. 3*A*) and human (Fig. 3*B*) complexes was significantly lower with $LA_{BC\Delta Ara}$, suggesting that the L-Ara4N modification of the lipid A plays a role in bioactivity of the LPS molecule.

Comparisons with NF-κB activation elicited by synthetic *E. coli*-type hexa-acylated lipid A revealed significantly less activation by LPS_{BC} and $LA_{BC\Delta Ara}$ (all at 50 ng/ml) (Figs. 3*A* and 3*B*). Lower activation by LPS_{BC} and $LPS_{BC\Delta Ara}$ could depend on weaker binding to MD-2 or less efficient activation of TLR4. Therefore, we examined whether LPS_{BC} and $LPS_{BC\Delta Ara}$ could interfere with TLR4 signaling elicited by the *E. coli* LPS by a competition assay in which HEK293 cells transfected with hTLR4/hMD-2 were pre-incubated with LPS_{BC} or $LPS_{BC\Delta Ara}$ for 1 h and then re-stimulated with *E. coli* LPS for 4 h (Fig. 4). Pre-incubation of cells with 10 ng/ml of LPS_{BC} followed by stimulation by 1 ng/ml of *E. coli* LPS, revealed weaker NF-kB activation than that with *E. coli* LPS alone ($P < 0.05$; Fig. 4). Interestingly, a two-fold reduction in NF-kB activation was evident in the case of pre-incubation with 10 ng/ml of $LPS_{BC\Delta Ara}$ ($P < 0.01$; Fig. 4). Further, a significant difference was found in activation by 10 ng/ml of *E. coli* LPS alone compared to that obtained after pre-incubation of cells with 100 ng/ml of LPS_{BC} and $LPS_{BC\Delta Ara}$ ($P < 0.01$; Fig. 4). In contrast, this

inhibitory effect was reduced by increasing the concentration of the pre-incubated LPS_{BC} and $LPS_{BC\Delta Ara}$ (100 ng/ml) added to the 1 ng/ml of *E. coli* LPS; such effect is probably due to the contribution of a weak activation of MD-2/TLR4 by LPS_{BC} and $LPS_{BC\Delta Ara}$. Collectively, these results suggest that $LPS_{BC\Delta Ara}$ efficiently binds to TLR4/MD-2 but is a weaker agonist compared to the *E. coli* LPS and LPS_{BC}.

The pro-inflammatory activity of LPS from *B. cenocepacia* was assessed using an established *in vivo* model of endotoxic shock. C57Bl/6 mice were challenged by intraperitoneal injection of LPS from *E. coli*, *P. aeruginosa* RP73 (a CF strain expressing penta- and tetra-acylated lipid A (37)), LPS_{BC} and $LPS_{BC\Delta Ara}$. After 5 h of treatment, TNF-α levels in sera were measured to evaluate pro-inflammatory and endotoxic potential. Compared to the saline solution control, penta-acylated LPS_{BC} induced robust TNF-α production (LPS_{BC} *vs* Ctrl $P < 0.01$; Fig. 5), while $LPS_{BC\Delta Ara}$ induced three-fold less systemic release of TNF-α in sera ($LPS_{BC\Delta Ara}$ *vs* LPS_{BC} $P < 0.01$, Fig. 5), suggesting a role for L-Ara4N residues in the endotoxic LPS response, also in agreement with the *in vitro* results (Fig. 2).

Identification of MD-2 amino acid residues involved in the interaction with LPS_{BC}–To further investigate the molecular recognition of LPS_{BC} and $LPS_{BC\Delta Ara}$ by TLR4/MD-2, we constructed targeted hMD2 and mMD-2 mutants that were co-expressed with hTLR4 or mTLR4 in transfected HEK293 cells. We focused on residues at the dimerization interface of the MD-2 protein (22,51). In particular, we examined valine-82 (Val82), located in the proximity to the pocket entrance at a loop between β-strands 5 and 6. This region contains several conserved, solvent-exposed hydrophobic residues that contribute to crucial hydrophobic interactions in the activated receptor complex (22). Val82 was replaced by phenylalanine (V82F) to augment the hydrophobic interactions of the MD-2/lipid A complex with TLR4. In comparison to HEK293 cells transfected with parental MD-2, hTLR4/hMD-2 V82F led to increased activation upon stimulation with LPS_{BC} and $LPS_{BC\Delta Ara}$, while *E. coli* LPS activation was not significantly modified (Fig. 6). This agrees with the notion that hexa-acylated lipid A provides stronger hydrophobic interactions with TLR4, and therefore increased hydrophobicity at position 82 augments the activation by penta-acylated LPS. No significant differences were detected between stimulation with LPS_{BC} and $LA_{BC\Delta Ara}$ on hTLR4/hMD-2 V82F. Hydrophobic interactions between mTLR4/mMD-2 and LA are expected to be similar to those involving the hTLR4/hMD-2 complex since nearly all the hydrophobic residues are conserved (51). However, the electrostatic interactions that contribute to receptor selectivity differ between mMD-2 and hMD-2 proteins. Particularly, hMD-2 has a positively charged lysine at position 122 near the pocket entrance, whereas mMD-2 has a negatively charged glutamic acid (51). Moreover, hMD-2 has a positively charged lysine at position 125, while mMD-2 has a hydrophobic leucine (51). In the complex, lysine residues 122 and 125 are close to the disaccharide backbone of LA (52) and are important for the species-specific differences in the recognition of lipid IV_A between hMD2 and mMD-2. We therefore introduced amino acid replacements at positions 122 and 125 in both MD-2 homologues to test whether the substitutions could affect LA binding and influence the selectivity of TLR4 activation by the LA_{BC} variants. The E122K replacement in mMD-2, introducing the equivalent lysine of hMD-2, had little or no effect on the activation induced by LA_{BC}, $LA_{BC\Delta Ara}$ or the hexa-acylated lipid A. In contrast, this replacement significantly decreased activation by lipid IV_A ($P < 0.001$; Fig. 7), likely due to removal of the repulsive forces towards its *bis*-phosphorylated disaccharide backbone. These repulsive interactions have been proposed to be important for positioning of lipid IV_A in an appropriate orientation for TLR4 dimerization (52). Thus, the unchanged LA_{BC}/$LA_{BC\Delta Ara}$ responsiveness suggests that the single residue at position 122 of the murine MD-2 protein is not critical for LA_{BC}/$LA_{BC\Delta Ara}$ signaling.

Stimulation of cells expressing the double E122K/L125K mMD-2 replacement (Fig. 7) showed substantially increased activity of the mutant MD-2 regardless of the LPS variant (Hexa-acylated lipid A *vs* Hexa-acylated lipid A $P < 0.05$, LA_{BC} *vs* LA_{BC} $P < 0.001$, $LA_{BC\Delta Ara}$ *vs* $LA_{BC\Delta Ara}$ $P < 0.001$ respectively on mTLR4/mMD-2 and mTLR4/mMD-2 E122K L125K; Fig. 7), except with lipid IV_A whose activity was strongly impaired ($P < 0.001$; Fig. 7). On the other hand, hMD-2 in combination with mTLR4 exhibited significantly stronger activation by $LPS_{BC\Delta Ara}$ ($P < 0.05$; Fig. 7), demonstrating that the L-Ara4N affects interaction with the TLR4 ectodomain. Moreover, the hMD-2 K122E mutant had an additive effect in combination with mTLR4 on the activation induced by $LA_{BC\Delta Ara}$, showing an increment of the NF-κB activity ($LA_{BC\Delta Ara}$ mTLR4/hMD-2 K122E *vs* $LA_{BC\Delta Ara}$ hTLR4/hMD-2 $P < 0.001$; $LA_{BC\Delta Ara}$ mTLR4/hMD-2 K122E *vs* $LA_{BC\Delta Ara}$ mTLR4/hMD-2 $P < 0.05$; Fig. 7). This probably reflects the presence of repulsive forces towards the phosphate groups of the lipid A, which might facilitate the orientation toward the Cys95/Cys105 loop (52,53).

Together, these experiments using hMD-2 and mMD-2 mutants support the notion that the peculiar structure of the LA_{BC} plays a key role in its interaction with MD-2, as well as in the dimerization process. Our data suggest that the L-Ara4N molecules on the di-glucosamine backbone influence the binding of lipid A to the TLR4/MD-2 complex, although their absence is not sufficient to impair signaling.

Molecular modeling of LPS_{BC} binding to TLR4/MD-2–Our previous results suggested that different MD-2 binding affinities drive the agonist activity of LPS. To provide a model for the interactions of LPS_{BC} and $LPS_{BC\Delta Ara}$, docking calculations were undertaken and the two ligands were docked into hMD-2 and mMD-2 proteins. Validation of the docking protocols was performed with AutoDock and AutoDock Vina by docking *E. coli* lipid A into the MD-2 protein from their corresponding crystallographic structures (PDB codes 3fxi –human and 3vq2 –murine). Values of root-mean-square deviation and predicted free energy of binding values indicated an excellent performance of both programs in predicting the crystallographic binding pose for both hMD-2 and mMD-2 proteins (Table 1).

LA_{BC} and $LA_{BC\Delta Ara}$ were predicted to bind both MD-2 homologues with binding poses that agreed with the crystallographic binding poses for *E. coli* lipid A (superimposition with *E. coli* lipid A in Figs. 8 and 9). Docking poses consisted of four fatty acid chains deeply immersed into the hydrophobic pocket of MD-2, establishing van der Waals and CH-π interactions with the side chains of most of the lipophilic residues of the MD-2 pocket, mainly consisting of aliphatic Leu, Ile and Val residues, aromatic Phe (numbering 76, 104, 119, 121, 126, 147, and 151), and Tyr (numbering 102, and 131) residues. All docked poses were found to participate in hydrophobic interactions with most of these residues. Higher efficiency in establishing lipophilic interactions can be deduced given the length of these four fatty acid chains. The fifth chain is placed into the groove or channel defined by Phe126, Leu87, Val82 and Arg90. This channel has been identified in the X-ray structures of the complex of TLR4/MD-2 with *E. coli* lipid A (18) as the allocation site for one lipid chain, allowing to complete the hydrophobic interface required for dimerization with the second TLR4/MD-2/ligand partner (referred to here as TLR4*/MD-2*). This precludes formation of the activated TLR4/MD-2/ligand multimer. Also Phe126 has been proposed as a switch controlling the agonist/antagonist conformation of MD-2, since Phe126 mutation prevents dimerization and abolishes downstream signaling (18,53).

Therefore, the model predicts that higher length of the five fatty acid chains compared to *E. coli* lipid A places the fifth chain outside the MD-2 pocket, thus building the dimerization interface in the Phe126, Leu87, Val82 and Arg90 groove, analogously to the sixth FA of *E. coli* lipid A, while the other four chains remain inside the MD-2 pocket, providing stabilizing interactions.

Further, the disaccharide scaffolds of LA_{BC} and $LA_{BC\Delta Ara}$, together with the phosphate groups, are predicted to be in the outer region and to establish electrostatic interactions with the polar residues which define the rim of the MD-2 pocket (Fig. 10) The higher predicted affinity for LPS_{BC} could be explained in terms of additional anchorage points arising from the L-Ara4N residues. In particular, these L-Ara4N molecules can establish additional interactions with MD-2. The hydroxyl (OH) group from Tyr102 establishes bridged H-bonding with the OH at position 2 of L-Ara4N and the OH from the acyl chain (Fig. 10), while OH at position 3 from the same L-Ara4N establishes a hydrogen bond with the Ser118 OH group. In the case of L-Ara4N 2, the OH group from one of the acyl chains establishes a hydrogen bond with Lys122 CO group, whereas OH-3 and ammonium groups, although out of the H-bond distance range (4.5 Å), are well oriented towards carbonyl groups from Lys122 and Gly123, may be enabling a putative H-bond networking at this site. These interactions could also be identified in the complex with the mMD-2 (data not shown). This predicted binding mode of LA_{BC} could thus explain the unexpected significant level of activation in the biological assays. The lack of some lipophilic interactions arising from the absent sixth fatty acid chain, in comparison to *E. coli* lipid A, could also be counterbalanced by these extra polar interactions from the L-Ara4N residues.

Molecular model of the hTLR4/MD-2 dimer in complex with LPS_{BC}–To develop a structural model for the TLR4/MD-2 dimer in complex with LPS_{BC} we first docked the inner core oligosaccharide moiety of LPS_{BC} (Fig. 1) on hTLR4, using as a guide the region where *E. coli* LPS inner core binds. The best binding pose was selected (theoretical binding free energy of -2.8 kcal mol^{-1}, by AutoDock Vina), taking also into account a proper orientation for the building of the full complex. The docked pose, superimposed with *E. coli* LPS core from PDB 3fxi, is shown in Fig. 11. The hTLR4/core complex was then assembled to the MD-2/LA_{BC} complex (best result from AutoDock Vina calculations), leading to a full hTLR4/MD-2/LPS_{BC} complex. The receptor dimer was built using PDB 3fxi as a template. The full 3D structure of the dimer complex (Fig. 12) was subjected to MDS, which did not show meaningful differences with the docked complexes (data not shown). The 3D model of the full complex supports the key interactions for the molecular recognition of LPS_{BC} that were described above and also confirms that the L-Ara4N residues (including the one present in the LPS core region, Fig. 1) play a fundamental role in the complex formation, as they participate in H-bonding at the dimerization interfaces (Fig. 13). First, both ammonium groups from L-Ara4N 2 and 3 (Fig. 13) (this latter is attached to a D-*glycero*-D-*talo*-2-octulosonic acid in the core moiety, Fig. 1) establish hydrogen bonds with the TLR4 Arg264 and Asp294 carboxylate groups. Second, the ammonium group of L-Ara4N 1 is close to the Asp395 carboxylate and the Ser416 OH group, which belong to the opposite TLR4*. Third, the OH-3 from L-Ara4N 1 establishes a H bond with Ser 415 CO group of TLR4* (Fig. 13). The 3D models from docking could suggest higher activation for LPS_{BC} *vs* $LPS_{BC\Delta Ara}$ arising from the extra anchorage points from arabinoses. This agrees with the higher endotoxic potential of LPS_{BC} in the biological assays. Based on this TLR4/MD-2/LPS_{BC} model, we have built a new model with the following four mutations: D294A, R322A, S415A*, and S416A*. These mutations involve the main residues establishing interactions with the ammonium groups from the three Ara4N residues, and the OH group from terminal glucose (Fig. 13): (i) D294 side chain establishes polar interactions reinforced by hydrogen bonds with the ammonium group from Ara4N-3, and is in the proximity of the ammonium group from Ara4N-2, so this residue can be considered as a main anchorage point for TLR4/MD-2/LPS_{BC}; Asp294 has been mutated to Ala to abolish this interaction; (ii) S415* and S416* are placed in the partner TLR4* and provide an anchorage point for ammonium group from Ara4N-1 through polar interactions with the side chain of S415* and the backbone CO groups; both Ser

residues have been mutated to Ala; (iii) although not directly contacting with any of the Ara4N moieties, R322 side chain establishes a hydrogen bond with the OH group at position 3 from the terminal glucose, and we mutated it to compare its contribution to the global energy of the system; this interaction is absent in the complex of TLR4/MD2 with *E. coli* LPS (PDB-ID 3fxi) and could be considered as a distinctive interaction for LPS_{BC} core. MDS and energy calculations of both systems (TLR4/MD-2/LPS_{BC} and mutant TLR4/MD-2/LPS_{BC}) have shown an important difference in the global energy: the wild type complex (TLR4/MD-2/LPS_{BC} model) is around 32 kcal mol^{-1} more stable than the mutant counterpart, mainly due to the coulombic term, pointing to the presence of important polar interactions (Table 2). Analysis of the contributions of each residue to the ligand binding energy reveals that this energy difference is mainly due to the lack of the interactions involving the mutated residues: (i) interaction with D294 is the highest interaction in the TLR4/MD-2/LPS_{BC} system (around 22 kcal mol^{-1}) and is absent in the mutant; (ii) also the interaction with R322 is missing, being one of the main interactions in the TLR4/MD-2/LPS_{BC} system (around 9.6 kcal mol^{-1}); (iii) the lower coulombic contribution to the interaction energy in the mutant TLR4/MD-2/LPS_{BC} complex is due to the absence of the interaction between the S415* side chain and the ammonium group. These results give reasonable evidences that the Ara4N ammonium groups provide additional anchorage interactions accounting for the final stability of the TLR4/MD-2/LPS_{BC} complex. Abolishing these interactions leads to a less stable complex, suggesting they are crucial for the binding.

DISCUSSION

Lipid A is a major determinant of cytokine induction in host immune cells (11-19,54). Generally, the highest immunostimulatory activity of lipid A correlates with its hexa-acylation pattern (11-19,54), since the sixth acyl chain protrudes from the MD-2 binding pocket bridging TLR4/MD-2 complex dimerization. On the contrary, underacylated lipid A molecules are not (or poorly) sensed by human TLR4/MD-2 being potentially accommodated within the MD-2 pocket. Here, we demonstrate a role for L-Ara4N residues in lipid A that explains why the *B. cenocepacia* LPS (naturally consisting of a mixture of penta- and tetra-acylated forms) acts as a strong TLR4/MD-2 agonist. Our results agree with a recent report by Hollaus *et al*. (36), demonstrating that a synthetic *Burkholderia* lipid A substituted with L-Ara4N exclusively at the anomeric phosphate acts as a potent human TLR4/MD-2 agonist.

Our *in vitro* and *in vivo* results explain and expand the above conclusions and show that *B. cenocepacia* penta-acylated lipid A (both LA_{BC} and $LA_{BC\Delta Ara}$) elicits an inflammatory response activating the TLR4/MD-2 complex, suggesting that the model of the receptor complex activation should also include other structural components. Further, molecular modeling experiments indicated that the increased length of the two amide-linked acyl chains of the *B. cenocepacia* lipid A moiety (3-(*R*)-hydroxyhexadecanoic acid C16:0 (3-OH) *vs* 3-(*R*)-hydroxytetradecanoic acid C14:0 (3-OH) from the *E. coli* lipid A) compensates the lack of one fatty acid chain filling the hydrophobic binding pocket of MD-2 protein, allowing the placement into the channel of the fifth acyl chain responsible for TLR4 dimerization. The replacement in *E. coli* lipid A of the secondary dodecanoic acid C12:0 with a hexadecanoic acid C16:0 results in a weaker LPS agonist (55). However, our data indicate not only the increased length of the acyl chain but also its position is important for agonist activity.

Further, our mutagenesis studies using two *B. cenocepacia* lipid A forms, LA_{BC} and $LA_{BC\Delta Ara}$, uncovered differential responsiveness on transfected HEK293 cells indicating an important role also for the L-AraN residues into the TLR4/LA_{BC} binding process. Particularly, the significantly different immunostimulatory activity of LA_{BC} compared to $LA_{BC\Delta Ara}$ (Fig. 7), observed in presence of the human MD-2 K122E mutation, might be related to the occurrence on LA_{BC} of the L-Ara4N residues, which could mask the negatively charged

phosphate groups and then reduce the repulsive forces introduced with the K122E mutation. In contrast, the absence of L-Ara4N in $LA_{BC\Delta Ara}$ might explain its increased agonistic activity when tested on HEK293 cells transfected with mTLR4/hMD-2 K122E, since the repulsive forces introduced might facilitate the orientation toward the Cys95/Cys105 loop (52-53). Therefore, it is reasonable to assume that the L-Ara4N-modification with its positively charged ammonium group could favor the electrostatic interactions allowing receptor/lipid A binding. Intriguingly, recent work by Maeshima *et al*. (56) revealed several key charged amino acid residues in TLR4 and MD-2 mediating host-specific responses to the glucosamine-modified penta-acylated lipid A from *B. pertussis* and its unmodified counterpart by human and mouse TLR4/MD-2 complexes. This further underscores the importance of positively charged residues decorating penta-acylated lipid A and interacting with human TLR-4/MD-2 charged amino acid residues to promote complex activation (56).

Our molecular modeling experiments further supported the notion that L-Ara4N residues provide additional polar interactions affecting the LA_{BC} binding to the TLR4/MD-2 and contribute to anchoring the lipid A into the receptor complex. The network of hydrogen bonds and polar interactions contributing to anchoring the lipid A into the TLR4/MD-2 involves not only the sugar residues from the core oligosaccharide (for example, hydrogen bonds involving Arg322, Fig. 13), but also the three L-Ara4N residues and the partner TLR4*. As stated above, mutagenesis studies demonstrate that several Lys residues involved in LPS binding play indispensable roles through the polar interactions with the phosphate groups (56-59). In our dimer model, Lys122 is involved in binding the lipid A moiety of the LPS_{BC} through polar interactions with the core; as for V82F, it has been already mentioned its role in building the groove that accommodates the acyl chain from lipid A, completing the interaction surface required for dimerization. The replacement of Val82 by phenylalanine involves changes of van der Waals interactions into CH-π interactions, which may favor the binding of this chain, longer than the corresponding one on *E. coli* LPS.

Thus, the structural peculiarities of *B. cenocepacia* i.e., its acylation pattern and the presence of the L-Ara4N residues in the lipid A region exert a synergistic effect in the activation and dimerization of the LPS receptor opening new insights into the comprehension of the molecular recognition of LPS by TLR4/MD-2.

Acknowledgements: We gratefully acknowledge financial support by Spanish MINECO (Grant CTQ2011-22724), Universidad CEU San Pablo (PC14/2011 and PC13/2012), Slovenian Research Agency, Centre of excellence EN-FIST, funded in part by the European structural funds, Cystic Fibrosis Canada, as well as COST actions BM1003 and CM1102, the Marie Curie ITN GLYCOPHARM PITN-GA-2012-317297 and H2020-MSCA-ITN-2014-ETN TOLLerant. ŁK thanks Airbus Military for a research contract. HEFCE Senior Lecturership and FFC grant support to ADS.

Conflict of interest: The authors declare that they have no conflict of interest with the content of this article.

Authors contributions: AM designed the research, FDL executed the chemistry and immunochemistry experiments, LK and SMS performed the MD experiments, all the authors have contributed with analytical tools or reagents or particular experiments, FDL, MAV, SMS and AM analyzed data and wrote the paper. All authors analyzed the results and approved the final version of the manuscript.

REFERENCES

1. Janeway, C. A., Jr, Medzhitov, R. (2002) Innate immune recognition. *Annu. Rev. Immunol.* **20**, 197-216.
2. Gay, N. J., Gangloff, M. (2007) Structure and function of Toll receptors and their ligands. *Annu. Rev. Biochem.* **76**, 141-165.
3. Broz, P., Monack, D. M. (2013) Newly described pattern recognition receptors team up against intracellular pathogens. *Nat. Rev. Immunol.* **13**, 551-65.
4. Nagai, Y., Akashi, S., Nagafuku, M., Ogata, M., Iwakura, Y., Akira, S., Kitamura, T., Kosugi, A., Kimoto, M., Miyake, K. (2002) Essential role of MD-2 in LPS responsiveness and TLR4 distribution. *Nat. Immunol.* **3**, 667-672.
5. Angus, D. C., Linde-Zwirble, W. T., Lidicker, J., Clermont, G., Carcillo, J, Pinsky, M. R. (2001) Epidemiology of severe sepsis in the United States: analysis of incidence, outcome, and associated costs of care. *Crit. Care Med.* **29**, 1303-1310.
6. Rangel-Frausto, M. S. (2005) Sepsis: Still going strong. *Arch. Med. Res.* **36**, 672-681.
7. Raetz, C. R. H., Whitfield, C., (2002) Lipopolysaccharide endotoxins. *Annu. Rev. Biochem.* **71**, 635-700.
8. Holst, O., Molinaro, A. (2009) Core oligosaccharide and lipid A components of lipopolysaccharides. In *Microbial Glycobiology: Structures Relevance and Applications*, Elsevier, San Diego, pp 29-56.
9. Knirel, Y. (2009) O-Specific polysaccharides of Gram-negative bacteria. In *Microbial Glycobiology: Structures Relevance and Applications*, Elsevier, San Diego, pp. 57-74.
10. Silipo, A., Erbs, G., Shinya, T., Dow, J. M., Parrilli, M., Shibuya, N., Newman, M. A., Molinaro, A. (2010) Glyco-conjugates as elicitors or suppressors of plant innate immunity. *Glycobiology* **20**, 406-419.
11. Brandenburg, K., Mayer, H., Koch, M. H., Weckesser, J., Rietschel, E. T., Seydel, U. (1993) Influence of the supramolecular structure of free lipid A on its biological activity. *Eur. J. Biochem.* **218**, 555-563.
12. Rietschel, E. T., Kirikae, T., Schade, F. U., Mamat, U., Schmidt, G., Schmidt, G., Loppnow, H., Ulmer, A. J., Zähringer, U., Seydel, U., Di Padova, F., Schreier, M., Brade, H. (1994) Bacterial endotoxin: molecular relationships of structure to activity and function. *FASEB J.* **8**, 217-225.
13. Brandeburg, K., Seydel, U., Schromm ,A. B., Loppnow, H., Koch, M. H. J., Rietschel, E. Th. (1996) Conformation of lipid A, the endotoxic centre of the bacterial lipopolysaccharide. *J. Endotoxin Res.* **3**, 173-178.
14. Seydel, U., Oikawa, M., Fukase, K., Kusumoto, S., Brandenburg, K. (2000) Intrinsic conformation of lipid A is responsible for agonistic and antagonistic activity. *Eur. J. Biochem.* **267**, 3032-3039.
15. Schromm, A. B., Brandenburg, K., Loppnow, H., Moran, A. P., Koch, M. H., Rietschel, E. T., Seydel, U. (2000) Biological activities of lipopolysaccharides are determined by the shape of their lipid A portion. *Eur. J. Biochem.* **267**(7), 2008-13.
16. Fukuoka, S., Brandenburg, K., Müller, M., Lindner, B., Koch, M. H., Seydel, U. (2001) Physico-chemical analysis of lipid A fractions of lipopolysaccharide from *Erwinia carotovora* in relation to bioactivity. *Biochim. Biophys. Acta* **1510**, 185-197.
17. Oikawa, M., Shintaku, T., Fukuda, N., Sekljic, H., Fukase, Y., Yoshizaki, H., Fukase K., Kusumoto, S. (2004) NMR conformational analysis of biosynthetic precursor-type lipid A: monomolecular state and supramolecular assembly. *Org. Biomol. Chem.* **2**, 3557-3565.
18. Park, B. S., Song, D. H., Kim, H. M., Choi, B. S., Lee, H., Lee, J. O. (2009) The structural basis of lipopolysaccharide recognition by the TLR4-MD-2 complex. *Nature* **458**, 1191-1195.
19. Maeshima, N., Fernandez, R.C. (2013) Recognition of lipid A variants by the TLR4-MD-2 receptor complex. *Front. Cell. Infect. Microbiol.* **3**, 3.
20. Golenbock, D. T., Hampton, R. Y., Qureshi, N., Takayama, K., Raetz, C. R. (1991) Lipid A-like molecules that antagonize the effects of endotoxins on human monocytes. *J. Biol. Chem.* **266**, 19490-19498.

21. Klett, J., Reeves, J., Oberhauser, N., Perez-Regidor, L., Martin-Santamaria, S. (2014) Modulation of toll-like receptor 4. Insights from x-ray crystallography and molecular modeling. *Curr. Top Med. Chem.* **14**(23), 2672-83.
22. Resman, N., Vašl, J., Oblak, A., Pristovšek, P., Gioannini, L., Weiss, J. P., Jerala, R. (2009) Essential roles of hydrophobic residues in both MD-2 and toll-like receptor 4 in activation by endotoxin. *J. Biol. Chem*. **284**, 15052-15060.
23. Ohto, U., Fukase, K., Miyake, K., Satow, Y. (2007) Crystal structures of human MD-2 and its complex with antiendotoxic lipid IV_A. *Science* **316**(5831), 1632-4.
24. Ernst, R. K., Yi, E. C., Guo, L., Lim, K. B., Burns, J. L. Hackett, M., Miller, S. I. (1999) Specific lipopolysaccharide found in cystic fibrosis airway *Pseudomonas aeruginosa*. *Science* **286**(5444), 1561-5.
25. Lohmann, K. L., Vandenplas, M. L., Barton, M. H., Bryant, C. E., Moore, J. N. (2007) The equine TLR4/MD-2 complex mediates recognition of lipopolysaccharide from *Rhodobacter sphaeroides* as an agonist. *J. Endotoxin Res*. **13**(4), 235-42.
26. Saitoh, S., Akashi, S., Yamada, T., Tanimura, N., Kobayashi, M., Konno, K., Matsumoto, F., Fukase, K., Kusumoto, S., Nagai, Y., Kusumoto, Y., Kosugi, A., Miyake, K. (2004) Lipid A antagonist, lipid IV_A, is distinct from lipid A in interaction with Toll-like receptor 4 (TLR4)-MD-2 and ligand-induced TLR4 oligomerization. *Int. Immunol*. **16**, 961-969.
27. Hajjar, A. M., Ernst, R. K., Tsai, J. H., Wilson, C. B., Miller, S. I. (2002) Human Toll-like receptor 4 recognizes host-specific LPS modifications. *Nat. Immunol*. **3**, 354-359.
28. Herath, T. D. K, Darveau, R. P., Seneviratne, C. J., Wang, C.Y., Wang, Y., Jin, L. (2013) Tetra- and Penta-acylated Lipid A structures of *Porphyromonas gingivalis* LPS differentially activate TLR4-mediated NK-kB signal transduction cascade and Immuno-inflammatory response in human gingival fibroblasts. *PlosOne* **3**, e58496.
29. Speert, D. P. (2002) Advances in *Burkholderia cepacia* complex. *Paediatr. Respir. Rev*. **3**, 230-235.
30. Hamad, M. A., Di Lorenzo, F., Molinaro, A., Valvano, M. A. (2012) Aminoarabinose is essential for lipopolysaccharide export and intrinsic antimicrobial peptide resistance in *Burkholderia cenocepacia*. *Mol. Microbiol*. **85**(5), 962-974.
31. Ortega, X., Cardona, S. T., Loutet, S., Brown, A., Flannagan, R. S., Campopiano, D., Govan, J. R. W., Valvano, M. A. (2007) A putative gene cluster for aminoarabinose biosynthesis is essential for *Burkholderia cenocepacia* viability. *J. Bacteriol*. **189**, 3639-3644.
32. Zughaier, S. M., Ryley, H. C., Jackson, S. K. (1999) Lipopolysaccharide (LPS) from *Burkholderia cepacia* is more active than LPS from *Pseudomonas aeruginosa* and *Stenotrophomonas maltophilia* in stimulating tumor necrosis factor alpha from human monocytes. *Infect. Immun*. **67**(3), 1505-7.
33. De Soyza, A., Ellis, C. D., Khan, C. M., Corris, P. A., Demarco de Hormaeche, R. (2004) *Burkholderia cenocepacia* lipopolysaccharide, lipid A, and proinflammatory activity. *Am. J. Respir. Crit. Care Med*. **170**(1), 70-7.
34. Bamford, S., Ryley, H., Jackson, S. K. (2006) Highly purified lipopolysaccharides from *Burkholderia cepacia* complex clinical isolates induce inflammatory cytokine responses via TLR4-mediated MAPK signalling pathways and activation of NFkappaB. *Cell Microbiol*. **9**(2), 532-43.
35. Silipo, A., Molinaro, A., Ieranò, T., De Soyza, A., Sturiale, L., Garozzo, D., Aldridge, C., Corris, P. A., Khan, C. M., Lanzetta, R., Parrilli, M. (2007) The complete structure and pro-inflammatory activity of the lipooligosaccharide of the highly epidemic and virulent gram-negative bacterium *Burkholderia cenocepacia* ET-12 (strain J2315). *Chemistry Eur. J*. **13**(12), 3501-11.
36. Hollaus, R., Ittig, S., Hofinger, A., Haegman, M., Beyaert, R., Kosma, P., Zamyatina, A. (2015) Chemical synthesis of *Burkholderia* lipid A modified with glycosyl phosphodiester-linked 4-amino-4-deoxy-β-L-arabinose and its immunomodulatory potential. *Chem. Eur. J*. **21**, 1-14.
37. Di Lorenzo, F., Silipo, A., Bianconi, I., Lore', N. I., Scamporrino, A., Sturiale, L., Garozzo, D., Lanzetta, R., Parrilli, M., Bragonzi, A., Molinaro, A. (2014) Persistent cystic

fibrosis isolate *Pseudomonas aeruginosa* strain RP73 exhibits an under-acylated LPS structure responsible of its low inflammatory activity. *Mol. Immunol.* **63**, 166-175.
38. Jeukens, J., Boyle, B., Bianconi, I., Kukavica-Ibrulj, I., Tümmler, B., Bragonzi, A., Levesque, R. C. (2013) Complete Genome Sequence of Persistent Cystic Fibrosis Isolate *Pseudomonas aeruginosa* Strain RP73. *Genome Announc.* **1**(4):e00568-13.
39. Westphal, O. J., Jann, K. (1965) Bacterial lipopolysaccharides:extraction with phenol-water and further applications of the procedure. *Methods Carbohydr. Chem.* **5**, 83-91.
40. Kittelberger, R., Hilbink, F. J. (1993) Sensitive silver-staining detection of bacterial lipopolysaccharides in polyacrylamide gels. *Biochem. Biophys. Methods* **26**, 81-86.
41. Ortega, X., Silipo, A., Saldias, M. S., Bates, C. C., Molinaro, A., Valvano, M. A. (2009) Biosynthesis and structure of the *Burkholderia cenocepacia* K56-2 lipopolysaccharide core oligosaccharide: truncation of the core oligosaccharide leads to increased binding and sensitivity to polymyxin B. *J. Biol. Chem.* **284,** 21738-21751.
42. Suite 2012: Maestro, version 9.3, Schrödinger, LLC, New York, NY, 2012.
43. Gaussian 03, Revision E.01, Frisch, M. J.; Trucks, G. W.; Schlegel, H. B.; Scuseria, G. E.; Robb, M. A.; Cheeseman, J. R.; Montgomery, Jr., J. A.; Vreven, T.; Kudin, K. N.; Burant, J. C.; Millam, J. M.; Iyengar, S. S.; Tomasi, J.; Barone, V.; Mennucci, B.; Cossi, M.; Scalmani, G.; Rega, N.; Petersson, G. A.; Nakatsuji, H.; Hada, M.; Ehara, M.; Toyota, K.; Fukuda, R.; Hasegawa, J.; Ishida, M.; Nakajima, T.; Honda, Y.; Kitao, O.; Nakai, H.; Klene, M.; Li, X.; Knox, J. E.; Hratchian, H. P.; Cross, J. B.; Bakken, V.; Adamo, C.; Jaramillo, J.; Gomperts, R.; Stratmann, R. E.; Yazyev, O.; Austin, A. J.; Cammi, R.; Pomelli, C.; Ochterski, J. W.; Ayala, P. Y.; Morokuma, K.; Voth, G. A.; Salvador, P.; Dannenberg, J. J.; Zakrzewski, V. G.; Dapprich, S.; Daniels, A. D.; Strain, M. C.; Farkas, O.; Malick, D. K.; Rabuck, A. D.; Raghavachari, K.; Foresman, J. B.; Ortiz, J. V.; Cui, Q.; Baboul, A. G.; Clifford, S.; Cioslowski, J.; Stefanov, B. B.; Liu, G.; Liashenko, A.; Piskorz, P.; Komaromi, I.; Martin, R. L.; Fox, D. J.; Keith, T.; Al-Laham, M. A.; Peng, C. Y.; Nanayakkara, A.; Challacombe, M.; Gill, P. M. W.; Johnson, B.; Chen, W.; Wong, M. W.; Gonzalez, C.; and Pople, J. A.; Gaussian, Inc., Wallingford CT, 2004.
44. Suite 2012: MacroModel, version 9.9, Schrödinger, LLC, New York, NY, 2012.
45. Suite 2012: Impact version 5.8, Schrödinger, LLC, New York, NY, 2012.
46. Suite 2012: Schrödinger Suite 2012 Protein Preparation Wizard; Epik version 2.3, Schrödinger, LLC, New York, NY, 2012; Impact version 5.8, Schrödinger, LLC, New York, NY, 2012; Prime version 3.1, Schrödinger, LLC, New York, NY, 2012.
47. Goodsell, D. S., Morris, G. M., Olson, A. J. (1996) Automated docking of flexible ligands: Applications of AutoDock. *J. Mol. Recognit.* **9**, 1-5.
48. Trott, O., Olson, A. J. (2010) AutoDock Vina: improving the speed and accuracy of docking with a new scoring function, efficient optimization and multithreading. *J. Comput. Chem.* **31**, 455-461.
49. Morris, G. M., Huey, R., Lindstrom, W., Sanner, M. F., Belew, R. K., Goodsell, D. S., Olson, A. J. (2009) AutoDock4 and AutoDockTools4: Automated docking with selective receptor flexibility. *J. Comput. Chem.* **16**, 2785-91.
50. Klett, J., Núñez-Salgado, A., Dos Santos, H. G., Cortés-Cabrera, A., Perona, A., Gil-Redondo, R., Abia, D., Gago, F., Morreale, A. (2012) MM-ISMSA: An Ultrafast and Accurate Scoring Function for Protein-Protein Docking. *J. Chem. Theory Comput.* **9**, 3395-3408.
51. Meng, J., Drolet, J. R., Monks, B. G., Golenbock, D. T. (2010) MD-2 residues tyrosine 42, arginine 69, aspartic acid 122, and leucine 125 provide species specificity for lipid IV_A. *J. Biol. Chem.* **285**, 27935-27943.
52. Ohto, U., Fukase, K., Miyake, K., Shimizu, T., (2012) Structural basis of species-specific endotoxin sensing by innate immune receptor TLR4/MD-2. *Proc. Natl. Acad. Sci. U S A* **109**(19), 7421-6.
53. Kobayashi, M., Saitoh, S., Tanimura, N., Takahashi, K., Kawasaki, K., Nishijima, M., Fujimoto, Y., Fukase, K., Akashi-Takamura, S., Miyake, K. (2006) Regulatory roles for MD-2 and TLR4 in ligand-induced receptor clustering. *J. Immunol.* **176**, 6211-6518.

54. Molinaro, A., Holst, O., Di Lorenzo, F., Callaghan, M., Nurisso, A., D'Errico, G., Zamyatina, A., Peri, F., Berisio, R., Jerala, R., Jimenez-Barbero, J., Silipo, A., Martin-Santamaria, S. (2015) Chemistry of Lipid A: at the heart of innate immunity. *Chem. Eur. J.* **21**, 500-19.
55. Bainbridge, B. W., Coats, S. R., Pham, T. T., Reife, R. A., Darveau, R. P. (2006) Expression of a *Porphyromonas gingivalis* lipid A palmitylacyltransferase in *Escherichia coli* yields a chimeric lipid A with altered ability to stimulate interleukin-8 secretion. *Cell Microbiol*. **8**, 120-129.
56. Maeshima, N., Evans-Atkinson, T., Hajjar, A. M., Fernandez, R. C. (2015) *Bordetella pertussis* Lipid A recognition by Toll-Like Receptor 4 and MD-2 is dependent on distinct charged and uncharged interfaces. *J. Biol. Chem.* **290**(21), 13440-53.
57. Gruber, A., Mancek, M., Wagner, H., Kirschning, C. J., Jerala, R. (2004) Structural model of MD-2 and functional role of its basic amino acid clusters involved in cellular lipopolysaccharide recognition. *J. Biol. Chem*. **279**, 28475-28482.
58. Re, F., Strominger, J. L. (2003) Separate functional domains of human MD-2 mediate Toll-like receptor 4-binding and lipopolysaccharide responsiveness. *J. Immunol*. **171**, 5272-5276.
59. Visintin, A., Latz, E., Monks, B. G., Espevik, T., Golenbock, D. T. (2003) Lysines 128 and 132 enable lipopolysaccharide binding to MD-2, leading to Toll-like receptor-4 aggregation and signal transduction. *J. Biol. Chem*. **278**, 48313-48320.

FOOTNOTES

[1]Department of Chemical Sciences, University of Naples Federico II, Naples 80126, Italy.
[2]Department of Chemistry and Biochemistry, Universidad CEU San Pablo, Boadilla del Monte, Madrid 28668, Spain.
[3]Department of Biopharmaceutics and Pharmacodynamics, Medical University of Gdańsk, Gdańsk 80-416, Poland.
[4]Department of Biotechnology, National Institute of Chemistry, Ljubljana 1000, Slovenia.
[5]Centre of excellence EN-FIST, Ljubljana 1000, Slovenia.
[6]Infection and Cystic Fibrosis Unit, IRCCS - San Raffaele Scientific Institute 20132, Milan, Italy
[7]Department of Microbiology and Immunology, University of Western Ontario, London N6A 5C1, Canada.
[8]Applied Immunobiology and Transplantation Group, Institute of Cellular Medicine, University of Newcastle, Newcastle NE1 7RU, United Kingdom.
[9] Centre for Infection and Immunity, Queen's University Belfast, Belfast BT9 7AE, United Kingdom
[10] Current address: Department of Chemical and Physical Biology, Centre for Biological Research, CIB-CSIC, Madrid 28040, Spain.
* To whom correspondence should be addressed: Antonio Molinaro, Department of Chemical Sciences, University of Naples Federico II, 80126, Naples, Italy. Tel.: (0039) 081674123; Fax: (0039) 081674393; E-mail: molinaro@unina.it. Sonsoles Martín-Santamaría, Department of Chemical and Physical Biology, Centre for Biological Research, CIB-CSIC, 28040, Madrid, Spain. Tel.: (0034) 0918373112; Fax: (0034) 915360432; E-mail: smsantamaria@cib.csic.es

[11]The abbreviations used are: CF, cystic fibrosis; FA, fatty acid; LA, lipid A; L-Ara4N, 4-amino-4-deoxy-L-arabinose; LA_{BC}, *B. cenocepacia* lipid A; $LA_{BC\Delta Ara}$, *B. cenocepacia* lipid A lacking L-Ara4N; LPS, lipopolysaccharide; LPS_{BC}, *B cenocepacia* LPS; $LPS_{BC\Delta Ara}$, *B cenocepacia* LPS lacking L-Ara4N; MD-2, myeloid differentiation factor 2; MDS, molecular dynamics simulation; PAMP, pathogen-associated molecular pattern; TLR4, Toll-Like Receptor 4.

FIGURE LEGENDS

FIGURE 1. Structure of *Burkholderia cenocepacia* LPS inner core and lipid A. *B. cenocepacia* lipid A is heterogeneous, being composed of a mixture of penta- and tetra-acylated species (30,40). Lipid A fatty acids are two 3-(*R*)-hydroxthexadecanoic acids, two 3-(*R*)-hydroxytetradecanoic acids and one tetradecanoic acid (30,40). The dotted lines indicate the non-stoichiometric substitution.

FIGURE 2. LPS_{BC} activates the murine and human TLR4/MD-2 complexes. NF-κB activation upon stimulation of HEK293 mTLR4/mMD-2 and hTLR4/hMD-2 after 6 h with 5 ng/ml of LPS_{BC} and $LPS_{BC\Delta Ara}$. Stimulation for 6 h with *E. coli* LPS was used as control. The data are pooled from three independent experiments done in triplicate. Bars indicate standard deviation; significance was calculated in comparison to stimulation with *E. coli* LPS (**P* <0.05, ***P* <0.01, ****P* <0.001). Curly brackets indicate significance calculated comparing LPS_{BC} and $LPS_{BC\Delta Ara}$ (**P* <0.05, ***P* <0.01, ****P* <0.001).

FIGURE 3. Lipid A activation of murine and human TLR4/MD2-complexes. *A.* NF-κB activation upon stimulation of HEK293 mTLR4/mMD-2 after 6 h with LA_{BC} and $LA_{BC\Delta Ara}$. Stimulations for 6 h with *E. coli* LPS, hexa-acylated lipid A and lipid IV_A were used as controls. The data are pooled from three independent experiments done in triplicate. Bars indicate standard deviation; significance was calculated in comparison to stimulation with hexa-acylated *E. coli* lipid A (**P* <0.05, ***P* <0.01, ****P* <0.001); curly brackets indicate significance calculated comparing LPS_{BC} and $LPS_{BC\Delta Ara}$ (**P* <0.05, ***P* <0.01, ****P* <0.001). *B.* NF-κB activation upon stimulation of HEK293 hTLR4/hMD-2 after 6 h with LA_{BC} and $LA_{BC\Delta Ara}$. Stimulations for 6 h with *E. coli* LPS, hexa-acylated lipid A and lipid IV_A were used as controls. The data are pooled from three independent experiments done in triplicate. Bars indicate standard deviation; significance was calculated in comparison to stimulation with hexa-acylated *E. coli* lipid A (**P* <0.05, ***P* <0.01, ****P* <0.001); curly brackets indicate significance calculated comparing LPS_{BC} and $LPS_{BC\Delta Ara}$ (**P* <0.05, ***P* <0.01, ****P* <0.001).

FIGURE 4. *B. cenocepacia* $LPS_{BC\Delta Ara}$ effects on the *E. coli* LPS agonist activity. Assay on the potential antagonist activity of LPS_{BC} and $LPS_{BC\Delta Ara}$ on hexa-acylated *E. coli* LPS. NF-κB activation upon stimulation of HEK293 hTLR4 after 1 h with LPS_{BC} (1, 10 and 100 ng/ml) and $LPS_{BC\Delta Ara}$ (1, 10 and 100 ng/ml) and then exposed to *E. coli* LPS (1 and 10 ng/ml) for 4 h. The data are pooled from three independent experiments done in triplicate. Bars indicate standard deviation; significance was calculated in comparison to stimulation with *E. coli* LPS (1 and 10 ng/ml) (**P* <0.05, ***P* <0.01, ****P* <0.001).

FIGURE 5. Pro-inflammatory and endotoxic potential of LPS_{BC} in C57Bl/6 mice. From three mice to five per group were challenged via intraperitoneal injection with 300 µg/mouse of LPS from *E. coli*, *P. aeruginosa* RP73, LPS_{BC} and $LPS_{BC\Delta Ara}$. TNF-α levels in sera were quantified after 5 h of treatment. Treatment with sterile saline solution was used as control (Ctrl). The data are pooled from two independent experiments. Results are reported as mean±S.D. Statistical analysis was made for pair wise comparisons (**P* <0.05, ***P* <0.01, ****P* <0.001).

FIGURE 6. *B. cenocepacia* LPS acylation pattern is responsible for the NF-κB activation. NF-κB activation upon stimulation of HEK293 hTLR4/hMD-2 after 6 h with LPS_{BC} and $LPS_{BC\Delta Ara}$. Stimulation for 6 h with *E. coli* LPS was used as control. The same protocol was used to stimulate HEK293 hTLR4/hMD-2 V82F cells. The data are pooled from three independent experiments done in triplicate. Bars indicate standard deviation; significance was calculated in comparison to *E. coli* LPS (**P* <0.05, ***P* <0.01, ****P* <0.001).

FIGURE 7. Lys-122 and Lys-125 in the *B. cenocepacia* LPS signaling on murine and human TLR4/MD-2 complexes. NF-κB-luciferase reporter assay executed stimulating HEK293 hTLR4/hMD-2, HEK293 mTLR4/mMD-2 and mTLR4/hMD-2 after 6 h with LPS_{BC} and $LPS_{BC\Delta Ara}$. Stimulations for 6 h with *E. coli* LPS and with lipid IV_A were used as controls. The same protocol was used to stimulate HEK293 mTLR4/mMD-2 E1222K and HEK293 mTLR4/mMD-2 E122K L125K cells. The data are pooled from two independent experiments done in triplicate. Bars indicate standard deviation; statistical analysis was calculated for pair wise comparisons (**P* <0.05, ***P* <0.01, ****P* <0.001).

FIGURE 8. Predicted binding mode of the LPS_{BC} core to *h*TLR4/MD-2. Computational model from docking followed by MDS. LPS_{BC} docked to MD-2 is shown in CPK colors. Superimposed fatty acids chains from *E. coli* lipid A are shown in different colors. Some representative residues from the MD-2 binding site are represented with carbon atoms in green.

FIGURE 9. Predicted binding mode of the LPS_{BC} core to *h*TLR4/MD-2. Details of LPS_{BC} (CPK colours) docked to MD-2. Superimposed fatty acids chains from *E. coli* lipid A are shown with carbon atoms in blue.

FIGURE 10. Predicted binding mode of the LPS_{BC} core to *h*TLR4/MD-2. Detail of some H-bond interactions between the LPS_{BC} inner core and TLR4/MD-2 involving Tyr102. LPS_{BC} is represented in CPK colors and MD-2 protein is represented in green.

FIGURE 11. Superimposition of best dock results of LPS_{BC} core. The docking was obtained using AutoDock Vina (depicted in red) and *E. coli* LPS core from PDB 3fxi (depicted in green). TLR4 is not shown for the sake of clarity.

FIGURE 12. Predicted binding mode of the LPS_{BC} core to *h*TLR4/MD-2. Computational model from docking followed by MDS. *Left panel*) 3D Model of the dimer of LPS_{BC} core in complex with TLR4/MD-2. *Right panel*) Detail of the dimer of LPS_{BC} inner core in complex with TLR4/MD-2.

FIGURE 13. Predicted binding mode of the LPS_{BC} core to *h*TLR4/MD-2. Details of some interactions between the LPS_{BC} inner core and TLR4/MD-2 from the computational model.

Table 1. Theoretical free energy of binding for the docking calculations with AutoDock 4.2 and AutoDock Vina (in bold). Energy values are in kcal mol^{-1}. Root-mean-square deviation (RMSD) values are in Å.

	human MD-2	murine MD-2
LA_{BC}	-20.02/-**25.30**	-17.73/-**23.60**
$LA_{BC\Delta Ara}$	-18.22/-**18.60**	-13.09/-**17.20**
E. coli lipid A	-24.41/-**28.3** (RMSD = 0.282/**0.599**)	-24.73/-**27.9** (RMSD = 0.647/**0.394**)

Table 2. Analysis of the per residue contributions to the total ligand binding energy for both complexes TLR4/MD-2/LPS$_{BC}$ and the mutated TLR4/MD-2/LPS$_{BC}$ (D294A, R322A, S415A*, and S416A*). Energy calculations come from the MDS. Only the top 22 contributions are shown (top 20 in the case of the mutant). Residues from TLR4 are underlined. Residues from the partner TLR4 are also marked with *.

	WT TLR4/MD-2/LPS$_{BC}$ complex						**Mutated TLR4/MD-2/LPS$_{BC}$ complex**					
Residue	Coulombic	vdW	Desolv	Apolar	HBond	Total	Coulombic	vdW	Desolv	Apolar	HBond	Total
Asp294	**-23.8236**	**-0.3210**	**7.0629**	**-0.9545**	**-4.0000**	**-22.0362**	**interaction not present in the mutated complex**					
Arg362	-11.8934	-0.7918	0.7816	-0.4113	-2.0000	-14.3149	-12.0533	-0.6813	0.8190	-0.4471	-3.0000	-14.3627
Phe121	0.0130	-10.1848	0.5344	-0.6027	0.0000	-10.2401	0.0197	-10.1477	0.5580	-0.6261	0.0000	-10.1961
Lys362	-5.1955	-5.2246	1.0497	-0.4985	0.0000	-9.8689	-5.2429	-5.1940	1.0644	-0.5256	0.0000	-9.8981
Arg322	**-4.1694**	**-3.0209**	**1.4981**	**-0.3240**	**-3.5617**	**-9.5779**	**interaction not present in the mutated complex**					
Ser120	-3.1530	-7.4177	2.8502	-0.6139	-1.1234	-9.4577	-3.1426	-7.4262	2.8920	-0.6447	-1.0989	-9.4204
Ser118	-2.8535	-5.8601	1.9418	-0.4578	-1.0000	-8.2297	-2.8551	-5.8194	1.9806	-0.4812	-1.0000	-8.1751
Phe119	-1.5159	-6.4383	0.3843	-0.3698	0.0000	-7.9398	-1.4890	-6.4515	0.3876	-0.3904	0.0000	-7.9433
Ser415*	**-2.4352**	**-5.8271**	**1.9501**	**-0.4780**	**-0.3041**	**-7.0943**						
Ile124	-0.1801	-6.4039	0.3739	-0.4557	0.0000	-6.6657	-0.1810	-6.3430	0.3881	-0.4727	0.0000	-6.6086
Arg264	-1.1413	-5.5336	2.6335	-0.4594	-2.0000	-6.5008	-1.1644	-5.5411	2.6761	-0.4832	-2.0000	-6.5125
Phe440*	-0.1050	-5.6291	0.2835	-0.3229	0.0000	-5.7735	-0.0997	-5.6015	0.2967	-0.3374	0.0000	-5.7419
Ile117	-0.2575	-5.3521	0.2913	-0.3661	0.0000	-5.6844	-0.2411	-5.3782	0.3048	-0.3803	0.0000	-5.6949
Phe126	0.0689	-5.4883	0.4065	-0.4173	0.0000	-5.4302	0.0642	-5.5509	0.4229	-0.4337	0.0000	-5.4975
Tyr269	-0.5477	-5.1443	1.3327	-0.3411	-0.3869	-5.0874	-0.5489	-5.4268	1.4007	-0.3883	-0.2386	-5.2018
Ser415*							**-0.4672**	**-4.9035**	**0.9431**	**-0.3809**	**-0.2240**	**-5.0324**
Leu61	0.0348	-4.6148	0.4221	-0.3884	0.0000	-4.5462	0.0351	-4.5972	0.4323	-0.4004	0.0000	-4.5303
Arg90	-0.2914	-5.6957	2.2470	-0.3640	0.0000	-4.1041	-0.2934	-5.6883	2.2559	-0.3797	0.0000	-4.1056
Ile52	0.0059	-3.9534	0.1916	-0.2931	0.0000	-4.0491	0.0059	-3.9438	0.2011	-0.3046	0.0000	-4.0414
Ile80	0.0264	-3.6513	0.2132	-0.2699	0.0000	-3.6815	0.0263	-3.6317	0.2209	-0.2775	0.0000	-3.6619
Phe151	0.0061	-3.4402	0.2277	-0.2298	0.0000	-3.4362	0.0060	-3.4279	0.2354	-0.2380	0.0000	-3.4245
Arg122	-0.9785	-3.6363	1.4626	-0.2523	0.0000	-3.4046	-0.9571	-3.6698	1.4845	-0.2670	0.0000	-3.4095
Tyr131	0.0104	-3.4712	0.4052	-0.2474	0.0000	-3.3029	0.0099	-3.4703	0.4135	-0.2570	0.0000	-3.3039

Figure 1

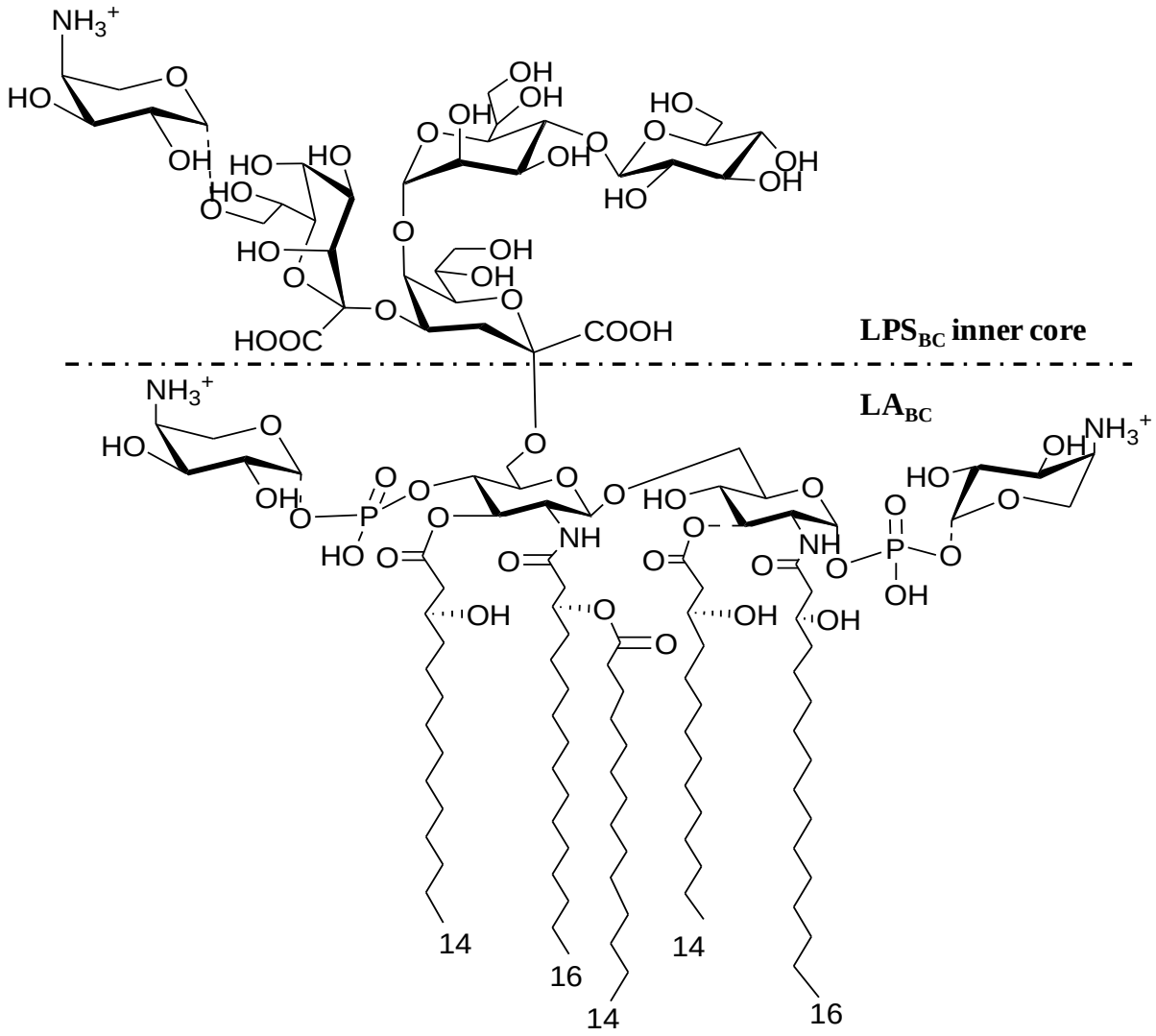

Figure 2

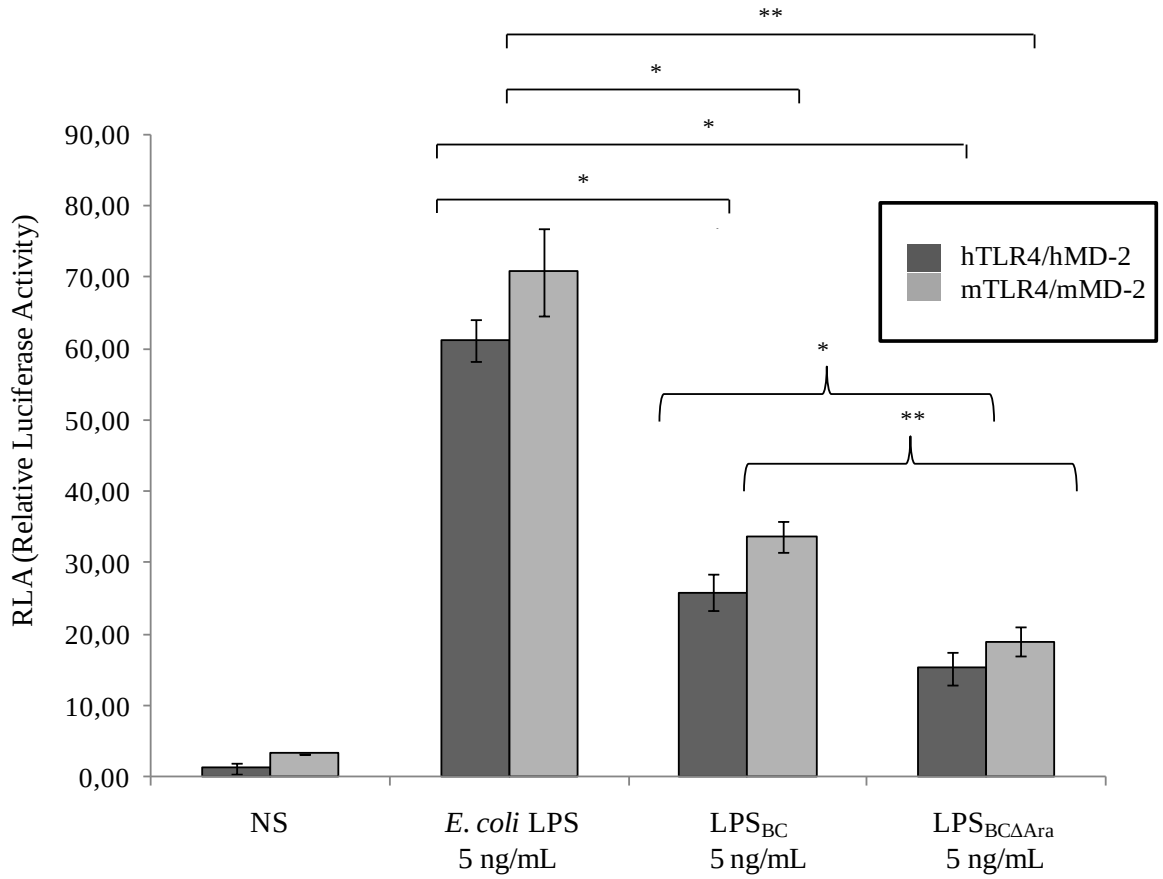

Figure 3*A*

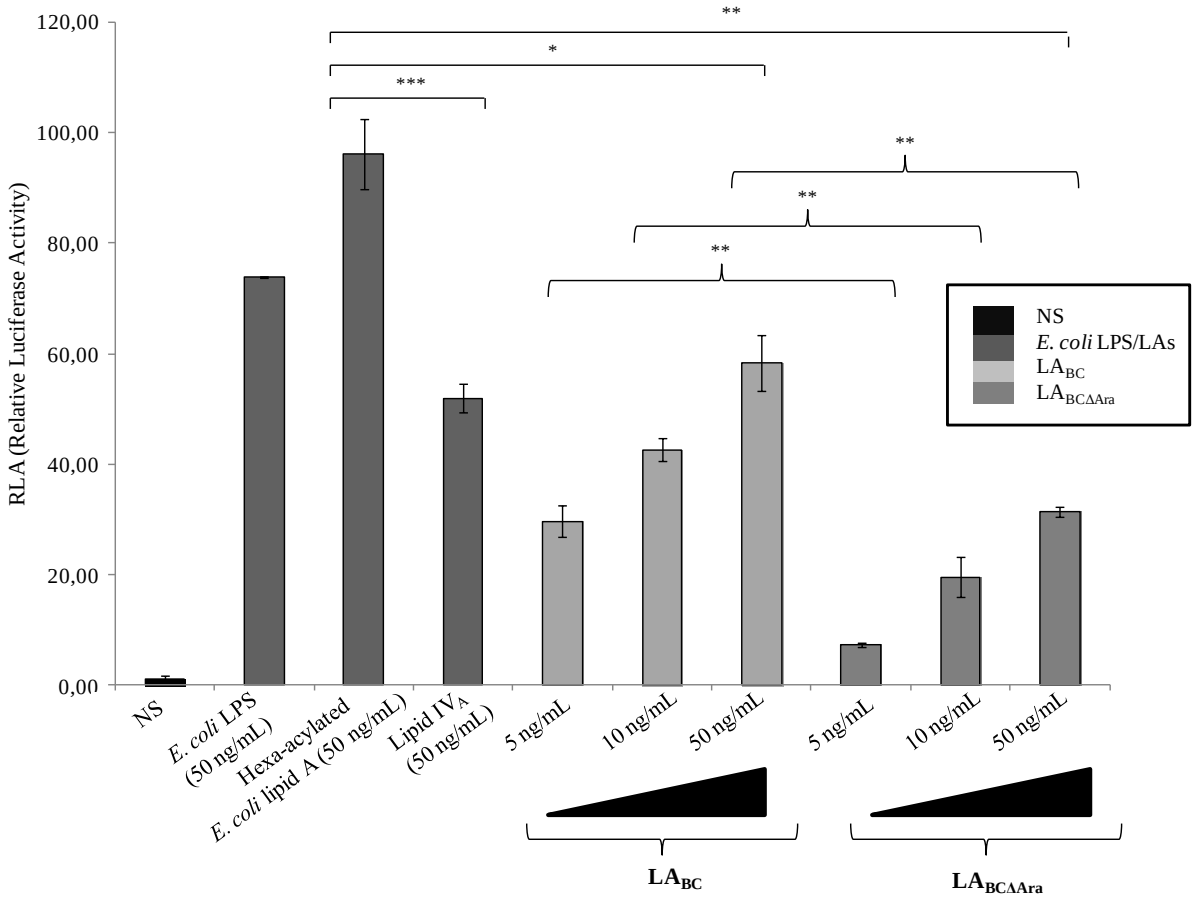

Figure 3*B*

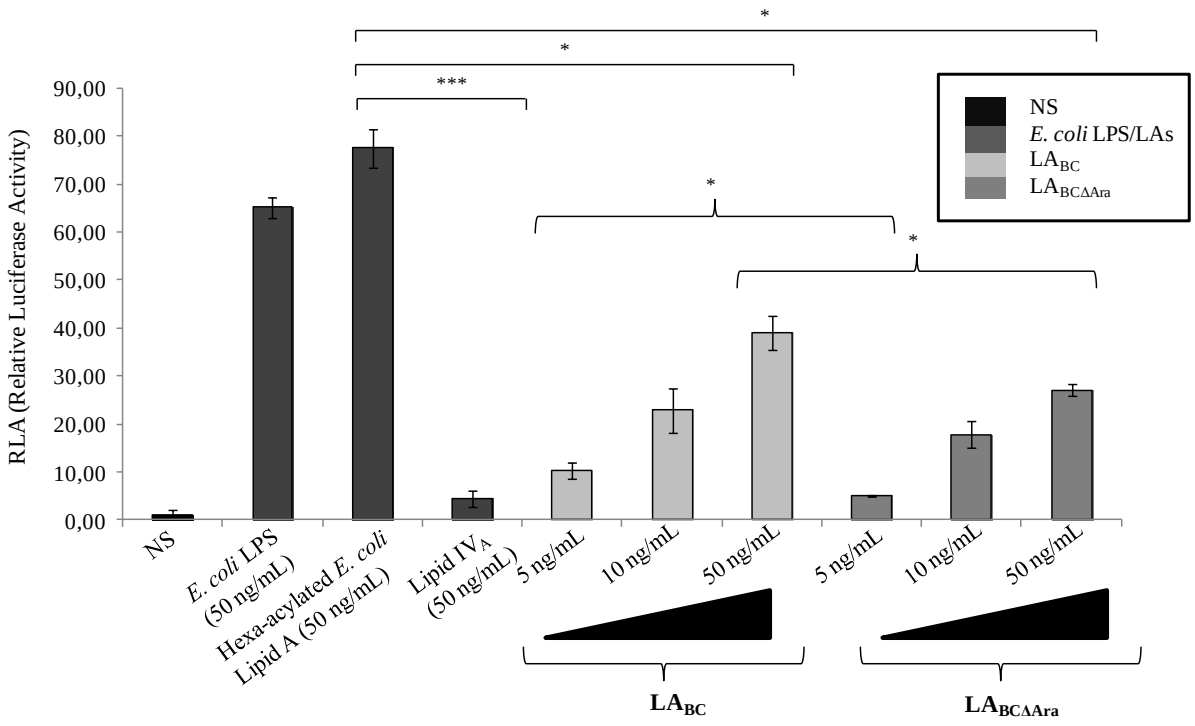

Figure 4

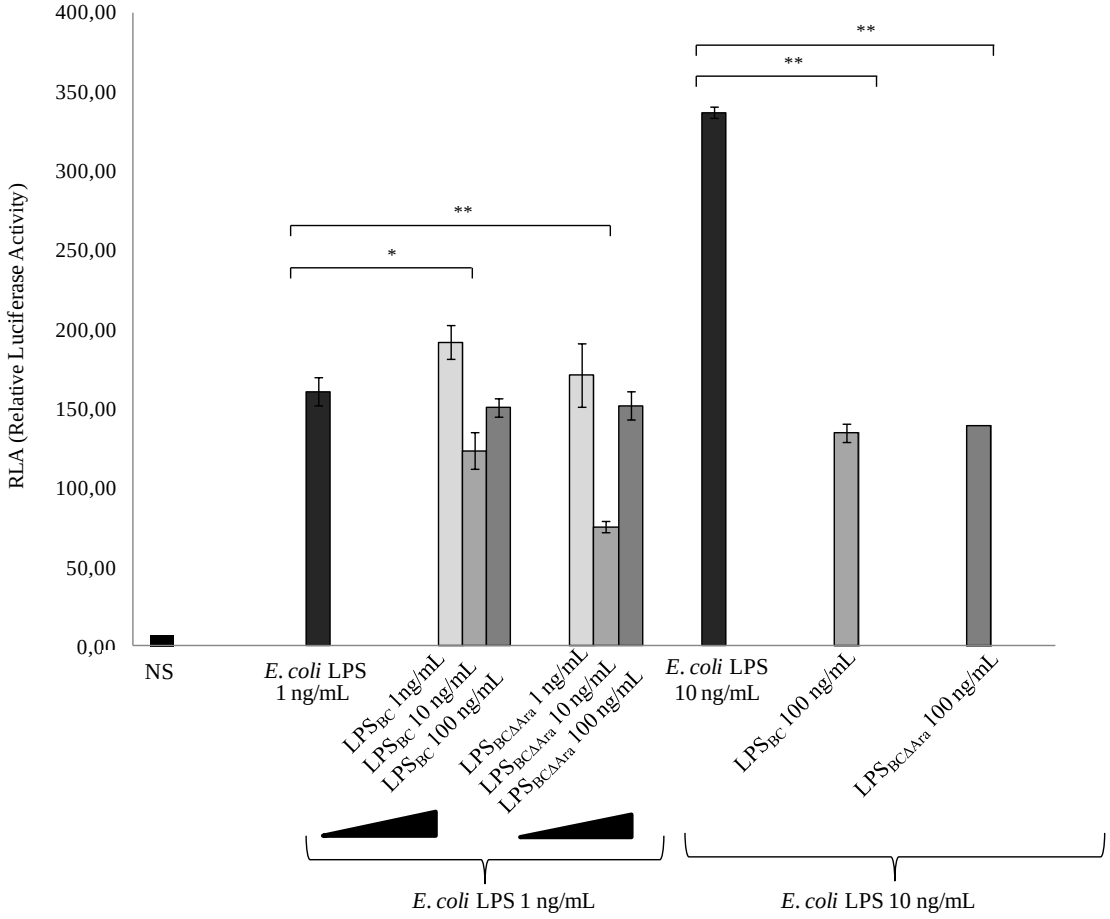

Figure 5

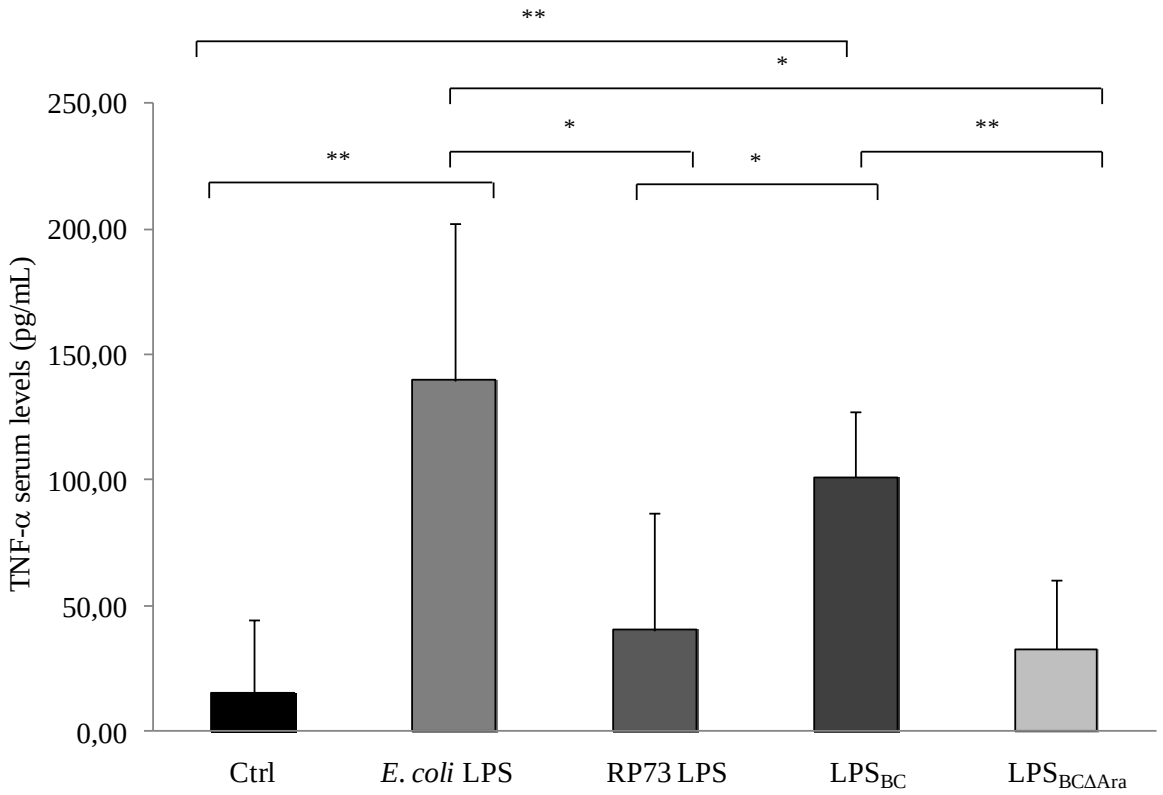

Figure 6

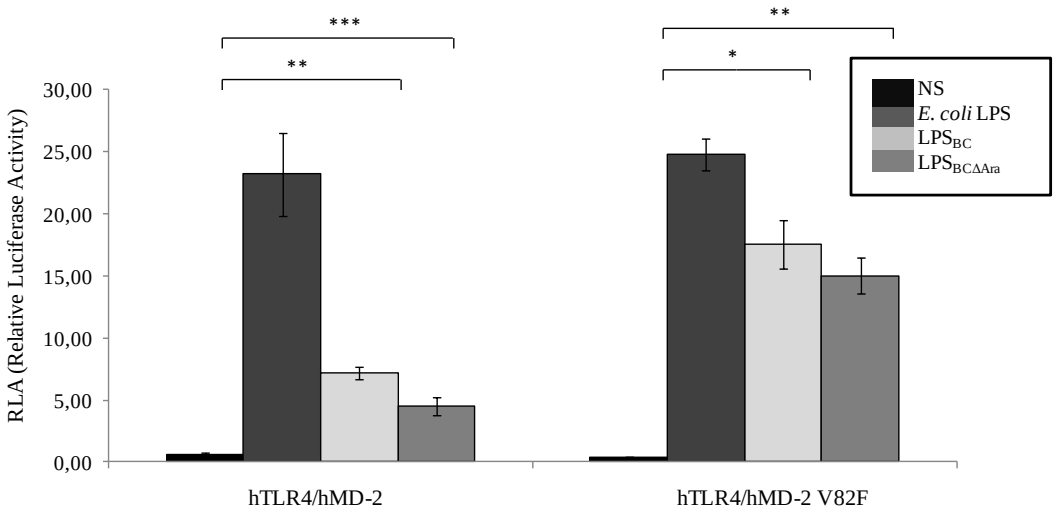

Figure 7

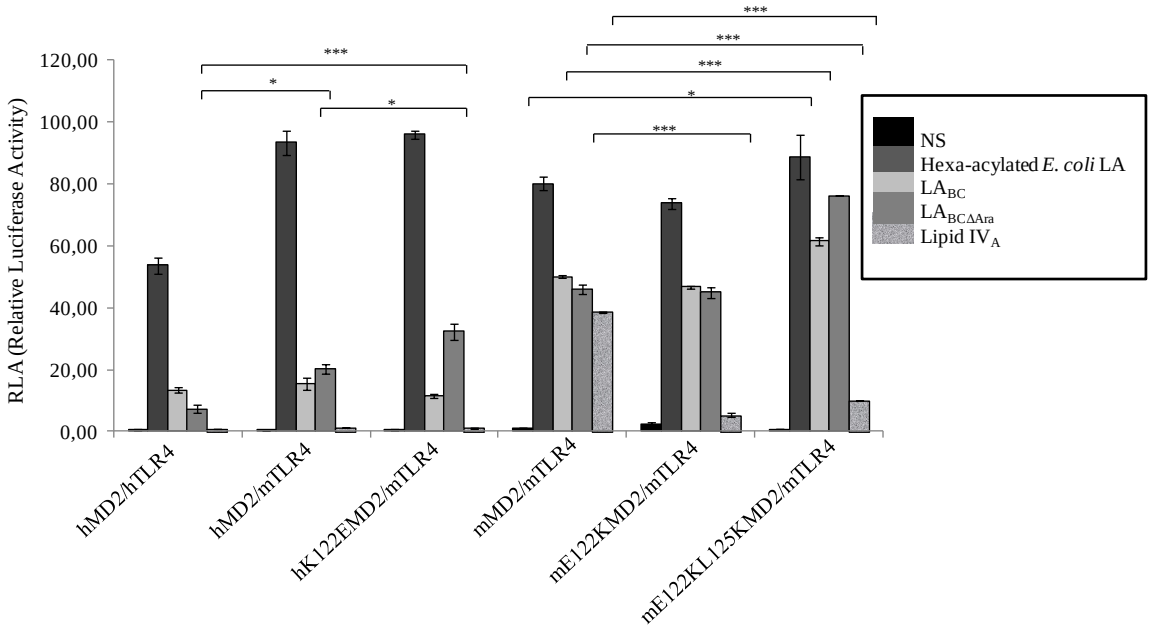

Figure 8

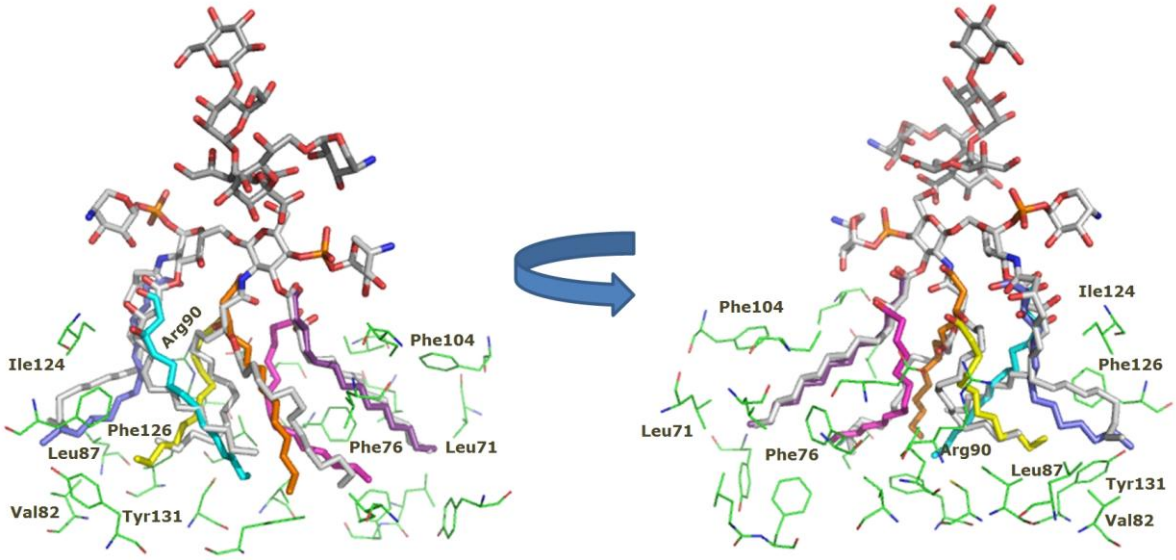

Figure 9

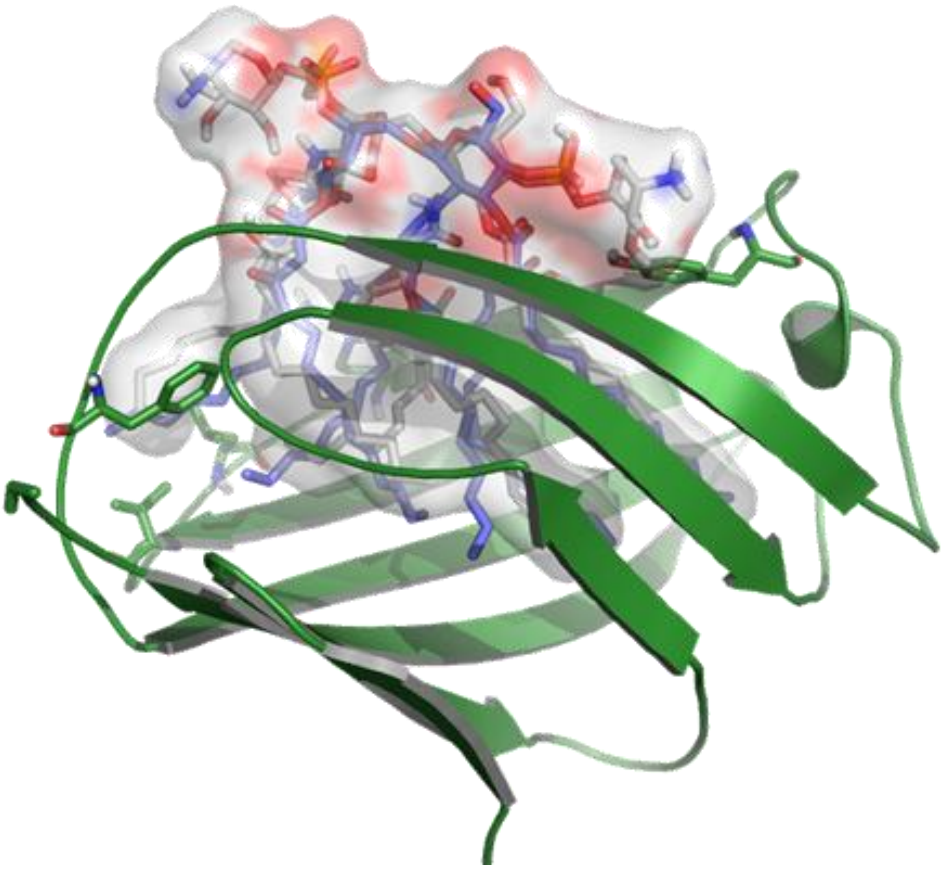

Figure 10

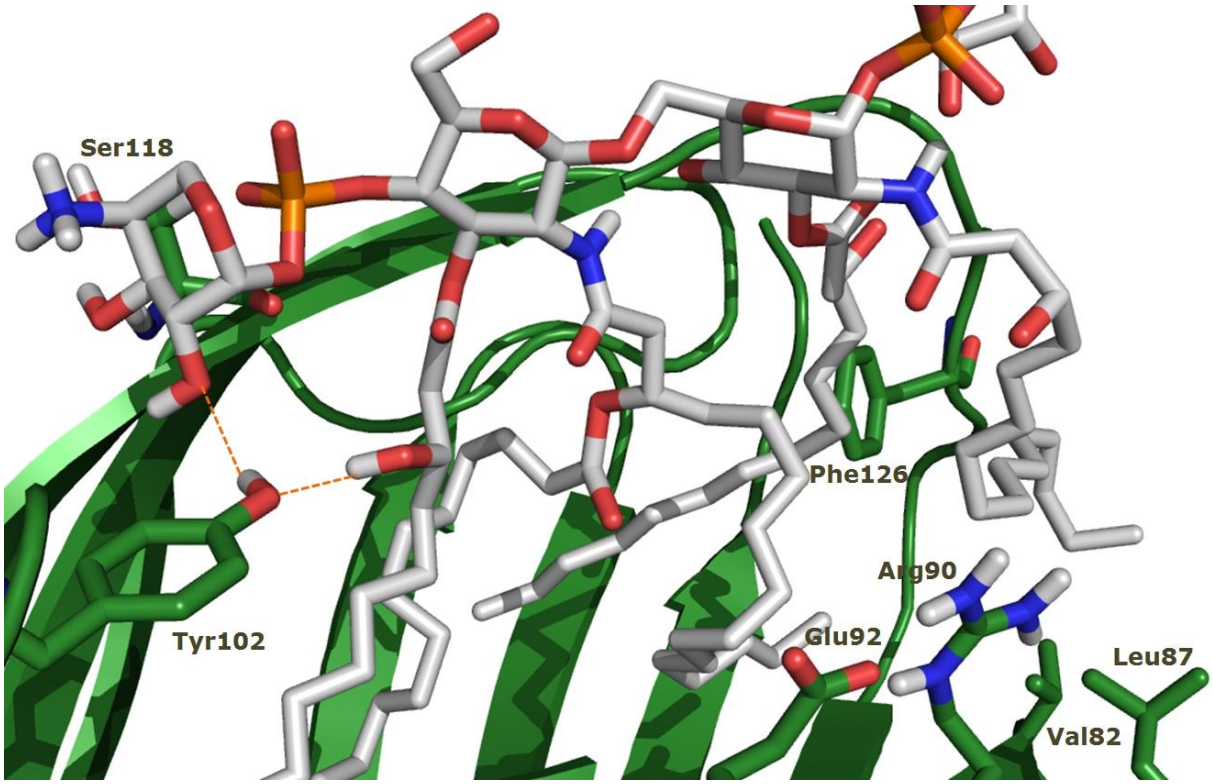

Figure 11

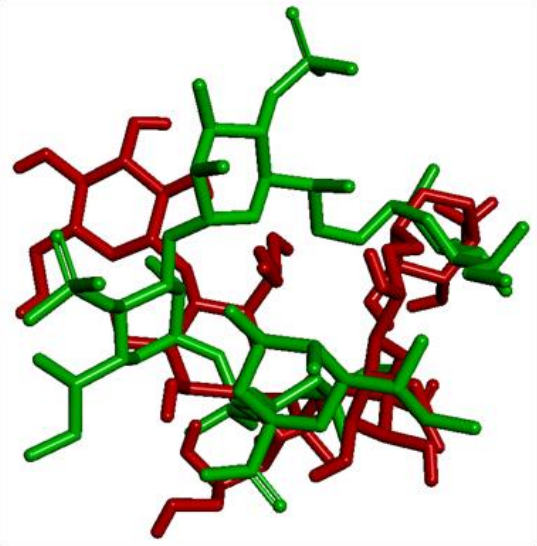

Figure 12

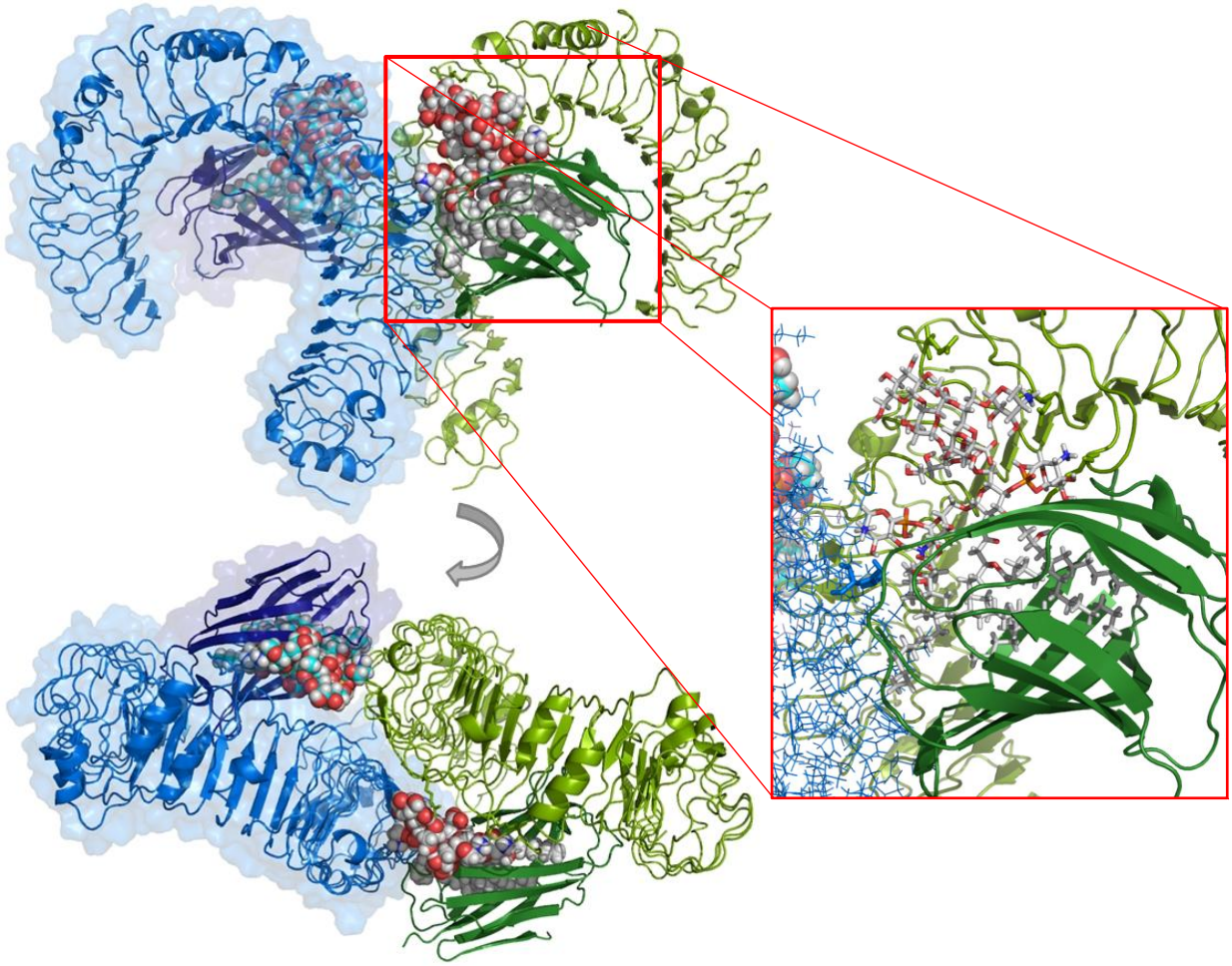

Figure 13

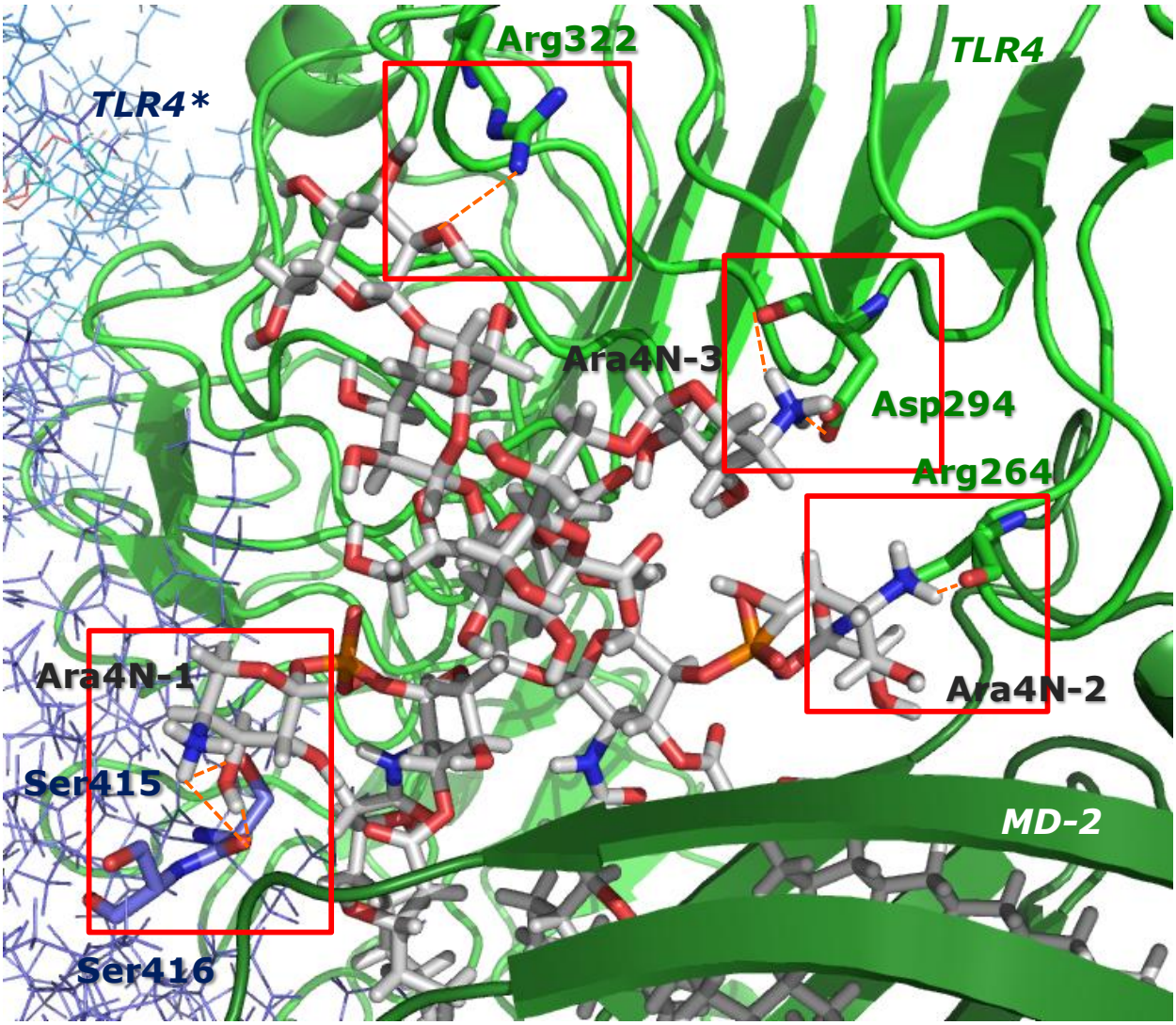

Glycobiology and Extracellular Matrices:

Activation of human TLR4/MD-2 by hypoacylated lipopolysaccharide from a clinical isolate of Burkholderia cenocepacia

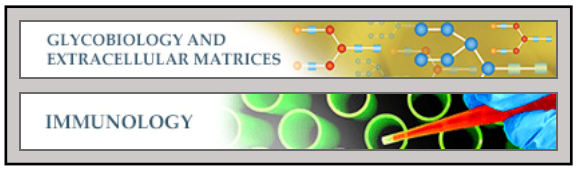

Flaviana Di Lorenzo, Lukasz Kubik, Alja Oblak, Nicola Ivan Lorè, Cristina Cigana, Rosa Lanzetta, Michelangelo Parrilli, Mohamad A. Hamad, Anthony De Soyza, Alba Silipo, Roman Jerala, Alessandra Bragonzi, Miguel A. Valvano, Sonsoles Martín-Santamaría and Antonio Molinaro

J. Biol. Chem. published online July 9, 2015